

# Scalability of Quasi-Hysteretic FSM-Based Digitally Controlled Single-Inductor Dual-String Buck LED Driver to Multiple Strings

Albert T. L. Lee, Johnny K. O. Sin, *Fellow, IEEE*, and Philip C. H. Chan, *Fellow, IEEE*

**Abstract**—There has been growing interest in single-inductor multiple-output (SIMO) dc–dc converters due to its reduced cost and smaller form factor in comparison with using multiple single-output converters. An application for such a SIMO-based switching converter is to drive multiple LED strings in a multichannel LED display. This paper proposes a quasi-hysteretic finite-state-machine-based digitally controlled single-inductor dual-output buck switching LED driver operating in discontinuous conduction mode (DCM) and extends it to drive multiple outputs. Based on the time-multiplexing control scheme in DCM, a theoretical upper limit of the total number of outputs in a SIMO buck switching LED driver for various backlight LED current values can be derived analytically. The advantages of the proposed SIMO LED driver include reducing the controller design complexity by eliminating loop compensation, driving more LED strings without limited by the maximum LED current rating, performing digital dimming with no additional switches required, and optimization of local bus voltage to compensate for variability of LED forward voltage  $V_F$  in each individual LED string with smaller power loss. Loosely binned LEDs with larger  $V_F$  variation can, therefore, be used for reduced LED costs.

**Index Terms**—Boundary conduction mode (BCM), discontinuous conduction mode (DCM), finite-state machine (FSM), single-inductor dual-output (SIDO), single-inductor multiple-output (SIMO).

## I. INTRODUCTION

A LED driver is essentially a current source (or sink) which maintains a constant current required for achieving the desired color and luminous flux from an array of LEDs. A number of highly efficient switching LED drivers have been reported in the literature and their primary objective is to achieve high power conversion efficiency [1]–[11]. Besides efficiency, another important consideration is the scalability of the existing single-inductor dual-output (SIDO) switching converter to drive multiple independent LED strings in a single-inductor multiple-output (SIMO) topology for reduced cost and smaller

form factor [12]. However, in practice, only a finite number of outputs can be served by each LED driver.

The prior arts of SIMO switching converter use either one of two ways to distribute energy from a single power supply to multiple outputs with a single inductor, namely multiple energizing phases [13]–[20] and single energizing phase per switching cycle [21]. The former with time-multiplexing control leads to much better suppression of cross regulation because the outputs are decoupled in time. In this paper, a quasi-hysteretic finite-state machine (FSM)-based digital control scheme is employed in a SIDO buck LED driver consisting of two independent parallel strings operating in discontinuous conduction mode (DCM). The extension of this SIDO architecture to SIMO is formally investigated. The proposed SIMO-based switching buck LED driver enables separate control of the three primary colors (red, green, and blue), thereby offering more flexibility for color mixing. The rest of this paper is organized as follows. Section II introduces the proposed quasi-hysteretic FSM-based digital controller for a SIDO switching buck LED driver operating in DCM. Section III provides a theoretical analysis on the scalability of the proposed digital control scheme from SIDO to SIMO and suggests a general formula for determining the theoretical upper bound in the total number of outputs in SIMO. Section IV shows Cadence Spectre simulation results that are used to verify the theoretical model. Section V contains the experimental results for the proposed digitally controlled SIDO buck LED driver. Section VI concludes our research effort.

## II. QUASI-HYSTERETIC FSM-BASED DIGITAL CONTROL FOR SIDO LED DRIVER

A SIDO switching converter with time-multiplexing control scheme operating in DCM was first reported in [13]–[16]. With such kind of time-multiplexing control scheme, a SIDO converter can easily be extended to drive multiple outputs and it exhibits negligible cross regulation in DCM. A SIMO parallel-string LED driver operating in DCM has recently been reported [12]. It uses an analog-based controller with dominant pole compensation for stability, and time-multiplexing control in DCM is employed to suppress cross regulation among the LED strings. Unlike conventional pulse width modulation (PWM)-based analog controllers, the proposed digital controller utilizing quasi-hysteretic control does not require any compensation circuits because of its inherent stability [22]–[24], hence simplifying the control loop design and reducing the component count and cost. Quasi-hysteretic control offers a good

Manuscript received November 7, 2012; revised January 22, 2013; accepted March 11, 2013. Recommended for publication by Associate Prof. J. M. Alonso.

A. T. L. Lee and J. K. O. Sin are with the Department of Electronic and Computer Engineering, The Hong Kong University of Science and Technology, Kowloon, Hong Kong (e-mail: alee@ust.hk; eesin@ust.hk).

P. C. H. Chan is with Hong Kong Polytechnic University, Hong Kong (e-mail: Philipch.Chan@inet.polyu.edu.hk).

Color versions of one or more of the figures in this paper are available online at <http://ieeexplore.ieee.org>.

Digital Object Identifier 10.1109/TPEL.2013.2253804

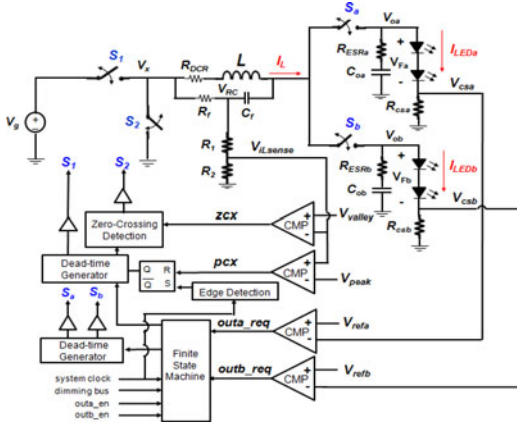


Fig. 1. System architecture of the quasi-hysteretic FSM-based digitally controlled SIDO buck LED driver.

85 compromise between traditional fixed-frequency PWM control  
 86 and pure hysteretic control with variable switching frequency.  
 87 In the proposed design, an external clock is used to synchron-  
 88 ize the buck LED driver which switches at a fixed frequency.  
 89 Fast comparators are used to control the on-time of the high-  
 90 side and low-side power switches by monitoring the inductor  
 91 current. This is particularly suitable for lighting applications  
 92 where variable switching frequencies are not desirable. The re-  
 93 configurable and scalability of a digital controller makes it  
 94 especially attractive for SIMO.

95 A major drawback of the previously proposed SIMO LED  
 96 driver operating in DCM [12] is that since the LED current is  
 97 discontinuous, the LED endures a higher maximum peak current  
 98 for the same average current required. In other words, the LED  
 99 could potentially be operating close to its absolute maximum  
 100 current rating, thereby increasing the current stress and possibly  
 101 shortening the operating lifetime of the LED. In their approach,  
 102 the LED current scales with the number of LED strings in SIMO.  
 103 Hence, the maximum current rating of the LED unnecessarily  
 104 restricts the maximum achievable number of LED strings which  
 105 can be implemented in SIMO. In the proposed design, the LED  
 106 current is always continuous and the LED can be regulated very  
 107 close to the target average current value which is much lower  
 108 than its maximum current rating. During the time interval when  
 109 the output switch is OFF, the output capacitor, acting as a con-  
 110 stant current source, continues to discharge its current to the  
 111 corresponding LED string. When the output switch is ON, the  
 112 power stage is reconnected to the LED string and the induc-  
 113 tor current is transferred to the output capacitor and the LED  
 114 string simultaneously. The current-sense feedback control en-  
 115 sures that the LED current is maintained at the desired dc level.  
 116 Hence, a time-continuous current is supplied to the LED string.  
 117 Consequently, the LED current does *not* scale with the number  
 118 of LED strings in the proposed SIMO architecture, making it  
 119 possible to drive more LED strings without inducing too much  
 120 stress on the LEDs. Fig. 1 shows the system architecture of the  
 121 proposed quasi-hysteretic FSM-based digitally controlled SIDO  
 122 buck switching LED driver which takes into account the parasitic  
 123 effects including the dc resistance (DCR) of the inductor  $L$

and equivalent series resistance (ESR) of the output capacitors  
 ( $C_{oa}, C_{ob}$ ). The two independently driven LED strings share  
 the same inductor  $L$  and the two main power switches ( $S_1, S_2$ )  
 of the buck converter. The output switches ( $S_a, S_b$ ) enable the  
 charge stored in the inductor to be distributed between the two  
 outputs in a time-multiplexed fashion. Dead-time generators  
 are used to eliminate shoot-through current by ensuring that  
 $S_1$  and  $S_2$  are not turned ON simultaneously. Dead-times are  
 also introduced between  $S_a$  and  $S_b$  to prevent inadvertent cross  
 conduction between the two LED strings.

Since an LED is essentially a current driven device, an LED  
 driver typically regulates the LED current rather than its forward  
 voltage. A straightforward way is to insert a small high-precision  
 current sensing resistor ( $R_{csa}, R_{csb}$ ) in series with the corre-  
 sponding LED string to sense the LED current by converting it  
 to the current-sense voltage ( $V_{csa}, V_{csb}$ ). The current-sense vol-  
 tage is then compared with the reference voltage ( $V_{refa}, V_{refb}$ ) to  
 generate the corresponding logic signals ( $outa\_req, outb\_req$ )  
 which determine the opening or closing of the two output  
 switches in a SIDO buck converter. Since the LED's  $I$ - $V$  curve  
 is usually provided by the LED manufacturer, the target dc cur-  
 rent value for a particular LED string can be set by choosing  
 an appropriate reference voltage. On the other hand, a two-limit  
 hysteretic control determines the on-time of the high-side and  
 low-side power switches ( $S_1, S_2$ ) of the buck converter. The  
 upper and lower limits of the inductor current, namely the peak  
 current limit and the valley current limit, define the average  
 value of the inductor current which is the *total* LED current for  
 a SIDO buck LED driver. In DCM, the valley current limit is  
 set to zero to prevent the inductor current from going negative  
 which degrades the power conversion efficiency [12], [16], [25].  
 As illustrated in Fig. 1,  $R_f C_f$  is connected in parallel to the  
 inductor so that the slopes of  $V_{RC}$  are proportional to the induc-  
 tor current ramp-up and ramp-down slopes [26]. A small  
 resistor ladder is connected between  $V_{RC}$  and ground in order  
 to generate a lower voltage signal  $V_{iLsense}$  which falls within  
 the input voltage range of the comparator (CMP).  $V_{iLsense}$  is  
 fed forward to the corresponding comparators to determine the  
 peak-crossing and zero-crossing of the inductor current. Fig. 2  
 is a simplified flowchart showing the system-level operation of  
 the proposed SIDO buck driver. Suppose identical current flows  
 through each of the two LED strings, also referred to as the  
*balanced load* condition, the inductor current  $I_L$  is assigned to  
 each string in alternate switching cycles. The working principle  
 of the proposed SIDO buck LED driver is represented by the  
 timing diagram shown in Fig. 3. During  $D_{1a}T_s$  or  $D_{1b}T_s$ ,  $I_L$   
 ramps up with a slope of  $m_1 = (V_g - V_o)/L$  and the inductor  
 is charged with a voltage of  $V_L = V_g - V_o$ , where  $V_g$  and  $V_o$   
 represent the input voltage and the output voltage, respectively.  
 During  $D_{2a}T_s$  or  $D_{2b}T_s$ ,  $I_L$  ramps down with a slope of  $m_2 =$   
 $-V_o/L$  and the inductor discharges its current to the correspond-  
 ing output capacitor and the LED string until  $I_L$  returns to zero.  
 During  $D_{3a}T_s$  or  $D_{3b}T_s$ ,  $I_L$  stays at zero with both  $S_1$  and  $S_2$   
 OFF. In the proposed SIDO LED driver, the system clock defines  
 the switching frequency. The rising edge of the system clock  
 triggers the ON duty cycle ( $D_{1a}T_s, D_{1b}T_s$ ) by charging  
 the inductor during which  $S_1$  is ON and  $S_2$  is OFF. The

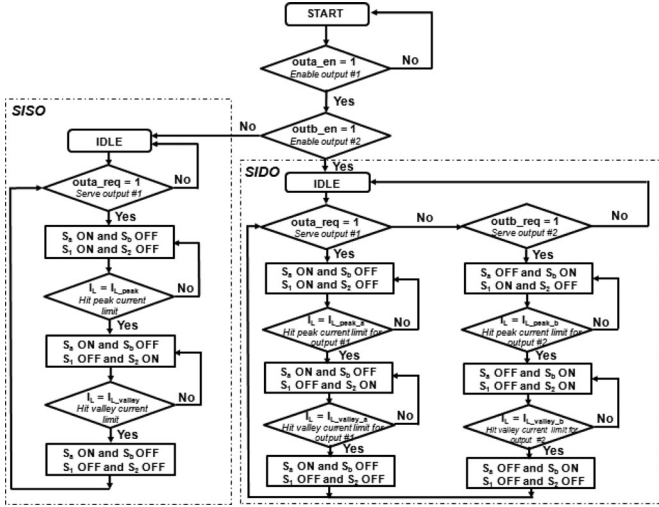


Fig. 2. Simplified flowchart representing the system-level operation of the proposed SIDO buck LED driver.

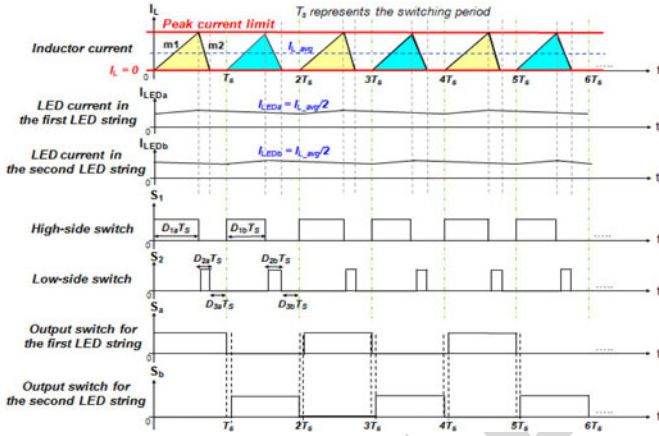


Fig. 3. Timing diagram of the proposed SIDO buck LED driver with balanced load operating in DCM.

181 inductor current continues to increase until it hits the peak  
 182 current limit at which point the buck converter enters  
 183 ( $D_{2a}T_s, D_{2b}T_s$ ) where  $S_1$  is OFF and  $S_2$  is ON. The inductor  
 184 discharges its current to the corresponding output until the  
 185 zero-crossing of the inductor current is detected. The converter  
 186 then enters the idle phase ( $D_{3a}T_s, D_{3b}T_s$ ) during which both  
 187  $S_1$  and  $S_2$  are OFF. The inductor current remains at zero until the  
 188 next rising edge of the system clock arrives and the switching  
 189 sequence repeats itself. The two output switches ( $S_a, S_b$ ) are  
 190 controlled by the FSM as shown in Fig. 4.

191 The state machine is triggered by the rising edge of the system  
 192 clock ( $sysclk$ ) so that the transitions of the output switches  
 193 ( $S_a, S_b$ ) are in sync with the system clock. The input signals  
 194 of the state machine are the output enable signals ( $outa\_en,$   
 195  $outb\_en$ ) and the output request signals ( $outa\_req, outb\_req$ )  
 196 which determine the switching sequence of the two outputs. The  
 197 first LED string is always given a higher priority over the second  
 198 one. For instance, if both strings request service simultaneously,  
 199 i.e.,  $outa\_req = 1$  and  $outb\_req = 1$ ,  $S_a$  is turned ON first and  
 200  $S_b$  remains OFF.  $S_b$  is turned ON only when  $outa\_req = 0$

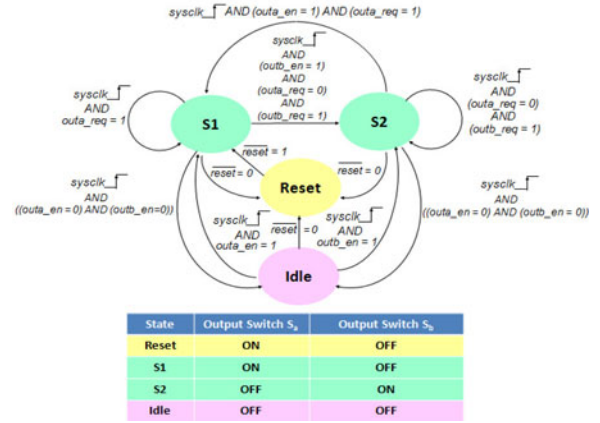


Fig. 4. State diagram of the proposed FSM for controlling the two output switches in SIDO buck LED driver.

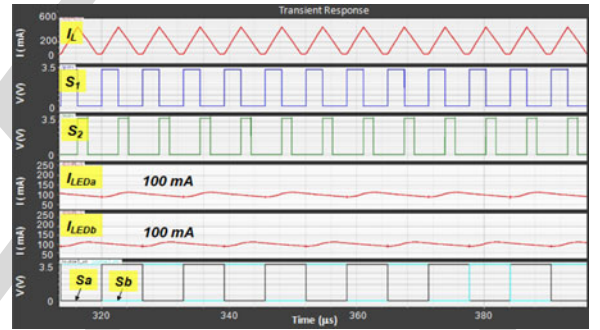


Fig. 5. Simulated steady-state waveforms for the proposed SIDO buck LED driver operating in DCM.

and  $outb\_req = 1$ .  $S_a$  and  $S_b$  must be nonoverlapping to avoid  
 201 undesirable cross conduction between the two LED strings. In  
 202 addition, an enable signal ( $out1en, out2en$ ) is associated with  
 203 either of the two LED strings. It provides the option of shutting  
 204 down any or all of the LED strings, for example, in response to an  
 205 overcurrent fault condition. An overriding signal can also be sent  
 206 from the FSM to the hysteretic controller to disable the high-side  
 207 and low-side power switches accordingly. The FSM-based controller  
 208 can be modified quickly and conveniently to drive multiple LED  
 209 strings in a SIMO configuration by simply adding more states in the  
 210 VHDL or Verilog code. A mixed-signal macromodel of the proposed  
 211 FSM-based digitally controlled SIDO buck switching LED operating in  
 212 DCM is simulated in the time domain using Cadence Spectre [27].  
 213 The FSM is modeled in Verilog RTL and the rest are modeled as  
 214 ideal circuit elements. The simulation model also incorporates  
 215 parasitics such as DCR of the inductor  $L$  and ESR of the output  
 216 capacitors ( $C_{oa}, C_{ob}$ ). For *balanced load* condition, the current  
 217 between the two LED strings is identical and each string consists  
 218 of *two* LEDs connected in series. First, the steady-state  
 219 performance is investigated. Fig. 5 contains the simulated  
 220 steady-state waveforms for the inductor current ( $I_L$ ), the LED  
 221 current ( $I_{LEDa}, I_{LEDb}$ ), and the four switches ( $S_1, S_2, S_a, S_b$ )  
 222 of the proposed SIDO buck LED driver operating in DCM. The  
 223 switching frequency is 156.25 kHz and the input voltage  $V_g$  is  
 224 15 V. The simulation results show that the LED current in either  
 225

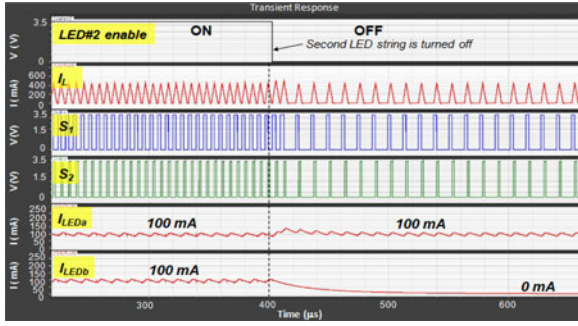


Fig. 6. First LED string remains under regulation without cross regulation when the second LED string is shut down completely.

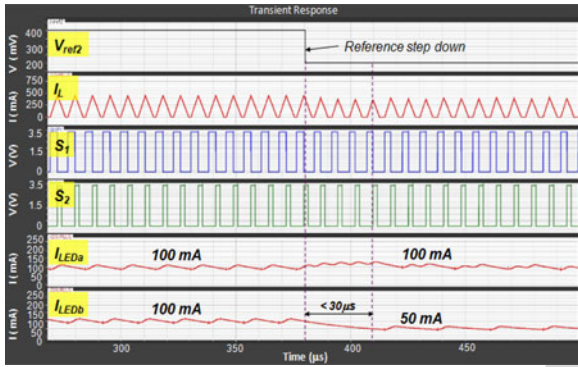


Fig. 7. First LED string remains under regulation without cross regulation despite a reference step in the second LED string from 100 to 50 mA in 20 ns.

of the two strings is regulated successfully to the target steady-state dc value of 100 mA with a current ripple of 23%<sub>P-P</sub>. The steady-state output voltage for the first and second LED string is approximately 6.48 V with a voltage ripple of 2.6%<sub>P-P</sub>. Second, the stability of the closed-loop system is verified by examining its dynamic performance. In the first scenario, the second LED string needs to be shut down instantly in response to an over-current condition. Fig. 6 shows that despite the immediate shutdown of the second LED string, the LED current  $I_{LEDa}$  in the first LED string continues to be regulated successfully at its target nominal value of 100 mA with minimal cross regulation. In the second scenario, the second LED string experiences a reference step of 50 mA, i.e.,  $I_{LEDb}$  transitions from 100 to 50 mA in 20 ns. Fig. 7 shows that the current in the first LED string continues to be regulated at around 100 mA, virtually unaffected by the sudden reference step in the other string. The second LED string settles to the new nominal current value of 50 mA. It demonstrates that the closed-loop system remains stable in response to the reference transient in the second string.

Unlike conventional backlight LED drivers that use PWM dimming transistor connected in series with the LED string [3], [8], [28]–[31], the proposed SIDO LED driver takes advantage of the existing four switches to perform dimming without requiring additional switches. When the dimming control signal for a particular LED string goes high, certain phases of the inductor current are skipped so that the average inductor current (also the average load current) going into that string is reduced accordingly. The digital dimming control signals ( $dim\_ctrl1$ ,

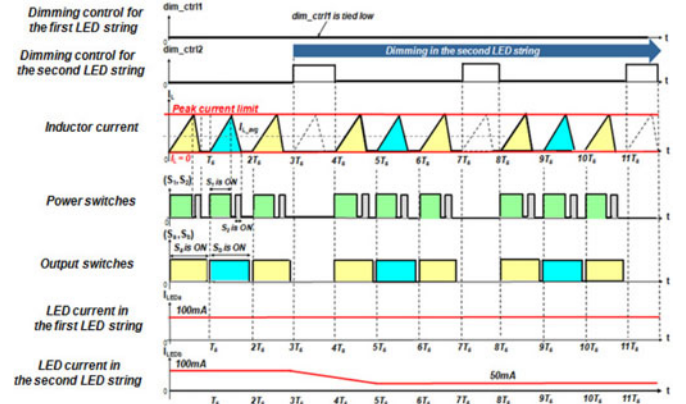


Fig. 8. Proposed digital dimming control in SIDO buck LED driver.

$dim\_ctrl2$ ) essentially modulate the dc current level flowing through the corresponding LED string. No additional dimming transistors in series with the LED string are required, thereby leading to a smaller voltage headroom and reduced power loss. The only voltage headroom is the voltage across the current-sense resistor ( $V_{csa}$ ,  $V_{csb}$ ) which is typically between 0.2 and 0.4 V. Fig. 8 depicts the timing diagram of the proposed digital dimming control scheme. In this particular case, the second LED string is dimmed by reducing its current from 100 to 50 mA, while the current in the first LED string stays constant at 100 mA.

Any combination of LED strings in a SIMO LED driver can be dimmed or even shut down momentarily to achieve flexible dimming and optimum luminance levels. In addition, it is reported in the literature [32]–[34] that a bilevel or  $N$ -level current driving technique for LED dimming improves the luminous efficacy of LEDs by introducing a dc offset to the PWM current. The proposed SIDO converter can potentially be used as a bilevel LED driver by generating two programmable dc current values for each individual LED string in a time-multiplexed fashion. Another major difference between the proposed LED driver and the existing ones [3], [8], [28]–[31] is that the former provides  $N$  optimized output bus voltage for each individual LED string, whereas the latter only uses a common output bus shared by all the LED strings. Due to manufacture, process, and temperature variations,  $V_F$  in each LED does not match perfectly, which means that the voltage drop across each LED string differs. Using the proposed SIDO buck LED driver in Fig. 1 as an example and assuming the LED current is 100 mA in each string, the voltage headroom ( $V_{csa}$ ,  $V_{csb}$ ) is 0.4 V, and the voltage drop across each of the two LED strings are  $V_{Fa} = 6.0$  V and  $V_{Fb} = 7.0$  V, respectively. The output voltages are  $V_{oa} = 6.4$  V and  $V_{ob} = 7.4$  V. The total power consumption of the load  $P_{LOAD}$ , including the LED string and current-sense resistor, is  $P_{LOAD} = V_{oa} \times I_{LED} + V_{ob} \times I_{LED} = 1.38$  W. The output voltage for each LED string is independently optimized based on its corresponding  $V_F$ , resulting in the same voltage headroom of 0.4 V for each string. This is different from a conventional LED driver in which the common output bus voltage is usually regulated using the LED string with the maximum voltage drop. For the same LED current, the total power consumption using a conventional LED driver is given by:  $P_{LOAD} =$

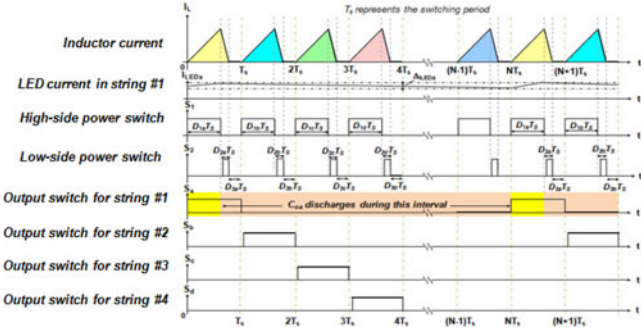


Fig. 9. Timing diagram of the proposed SIMO buck LED driver.

296  $2 \times \max(V_{oa}, V_{ob}) \times I_{LED} = 1.48 \text{ W}$ , which is more than 7%  
 297 higher than that of the proposed driver. The voltage headroom  
 298 for the first LED string increases from 0.4 to 1.4 V, resulting in  
 299 450 mW more power loss or additional 30% efficiency degra-  
 300 dation. Since the output voltage is self-optimized to match the  
 301 total  $V_F$  in each individual LED string in the proposed driver,  
 302 same-colored LEDs from neighboring bins (not only from a  
 303 single bin) with larger  $V_F$  variance can be used which helps  
 304 reduce the LED costs. In the event that a particular application  
 305 demands a total LED current greater than the average inductor  
 306 current, the same time-multiplexing control scheme operating  
 307 in DCM can still be employed either by lowering the switch-  
 308 ing frequency with a higher inductor peak current limit or by  
 309 operating the buck LED driver in pseudocontinuous conduc-  
 310 tion mode (PCCM) [17], [35], [36]. In PCCM, the average inductor  
 311 current is increased by simply adding a nonzero dc offset of  $I_{DC}$   
 312 to that of DCM.

### 313 III. EXTENSION FROM SIDO TO SIMO BUCK LED DRIVER

314 Having demonstrated the feasibility of the proposed SIDO  
 315 buck LED driver, it is natural for us to extend it to SIMO with  
 316  $N$  independently driven LED strings. In particular, the theo-  
 317 retical maximum number of LED strings  $N_{max}$  is determined  
 318 for this SIMO architecture. Fig. 9 shows a timing diagram of  
 319 the inductor current, the two power switches ( $S_1, S_2$ ), and the  
 320 first four output switches ( $S_a, S_b, S_c, S_d$ ) in a SIMO buck LED  
 321 driver. To simplify the analysis, the *balanced load* condition is  
 322 assumed. Based on the time-multiplexing control scheme, en-  
 323 ergy is being transferred from the dc supply to each individual  
 324 output *exactly once* within a total of  $N$  switching phases. For a  
 325 particular output, the corresponding output switch is OFF dur-  
 326 ing  $D_3$ , while the output capacitor discharges to the LED string.  
 327 During the subsequent  $(N - 1) \times T_s$  phases, the output switch  
 328 remains OFF and the output capacitor continues to discharge  
 329 to the corresponding LED string. Hence, the *total* discharging  
 330 time for the output capacitor  $t_{dch}$  can be expressed as

$$t_{dch} = D_3 T_s + (N - 1) T_s = (D_3 + N - 1) T_s. \quad (1)$$

$$\text{For } D_3 = 0, t_{dch} = (N - 1) T_s. \quad (2)$$

331 The proposed SIMO buck LED driver is essentially a  
 332 constant-current regulator which maintains a constant dc cur-  
 333 rent  $I_{LED}$  flowing through the LED string via a closed-loop

current-sense feedback control. For very small variation of for- 334  
 ward voltage around the quiescent point (also known as bias 335  
 point) on the LED's exponential  $I$ - $V$  curve, the dc forward cur- 336  
 rent is assumed to be constant. During  $t_{dch}$  when the output 337  
 switch is OFF, the output capacitor is connected to the LED 338  
 string which acts as a constant-current sink (CCS). Assuming 339  
 ideal capacitor with no ESR (the effect of the ESR will be ex- 340  
 plained later), the voltage across the output capacitor  $v_c(t)$  is the 341  
 same as the output voltage which is expressed as the charge  $q(t)$  342  
 divided by the capacitance value  $C_o$ , i.e., 343

$$v_c(t) = \frac{q(t)}{C_o} = \frac{1}{C_o} \int_0^{t_{dch}} i_c(\tau) d\tau + v_c(0). \quad (3)$$

$$\text{For CCS, } i_c(\tau) = I_{LED}. \quad (4)$$

Combining (3) and (4) and rearranging, we have 344

$$\Delta v_o = \Delta v_c = v_c(t) - v_c(0) = \frac{1}{C_o} (I_{LED} t_{dch}). \quad (5)$$

Hence, the *total* discharging time  $t_{dch}$  can be expressed as 345

$$t_{dch} = \frac{C_o \Delta v_o}{I_{LED}} \quad (6)$$

where  $\Delta v_o$  is the output voltage drop due to the discharging 346  
 of the output capacitor. In general,  $\Delta v_o$  is assumed to be 347  
 reasonably small relative to the output voltage. The LED ripple 348  
 current  $\Delta i_{LED}$  usually ranges from 10%<sub>P-P</sub> to 40%<sub>P-P</sub> of the 349  
 dc forward current as recommended by the LED manufactur- 350  
 ers [37], [38]. For a particular  $\Delta i_{LED}$ , the corresponding voltage 351  
 ripple  $\Delta v_{LED}$  at the chosen bias point can be readily obtained 352  
 from the exponential  $I$ - $V$  curve. Suppose each LED string con- 353  
 tains a total of  $n$  LEDs connected in series. The output voltage 354  
 ripple  $\Delta v_o$  is, therefore, the sum of the voltage ripple across 355  
 the LED string and the voltage ripple across the current-sense 356  
 resistor, i.e.,  $\Delta v_o = n \times \Delta v_{LED} + \Delta v_{cs}$ . Suppose  $\Delta v_{o,max}$  rep- 357  
 represents the *maximum* output voltage ripple allowed. Equation (6) 358  
 can, therefore, be rewritten as 359

$$t_{dch} \leq \frac{C_o \Delta v_{o,max}}{I_{LED}}. \quad (7)$$

Substituting (1) into (7), we have 360

$$\begin{aligned} (D_3 + N - 1) T_s &\leq \frac{C_o \Delta v_{o,max}}{I_{LED}} \Rightarrow N \\ &\leq \frac{C_o \Delta v_{o,max}}{I_{LED} T_s} + 1 - D_3. \end{aligned} \quad (8)$$

Hence, the theoretical maximum possible number of LED 361  
 strings in SIMO,  $N_{max}$ , is given by 362

$$N_{max} = \frac{C_o \Delta v_{o,max}}{I_{LED} T_s} + 1 - D_3 = \frac{C_o \Delta v_{o,max}}{I_{LED} T_s} + D_1 + D_2. \quad (9a)$$

Since  $N_{max}$  is an integer value, the *floor*( $\cdot$ ) function is used to 363  
 round the result down to the closest integer. Hence, (9a) becomes 364

$$N_{max} = \text{floor} \left( \frac{C_o \Delta v_{o,max} + I_{LED} T_s (1 - D_3)}{I_{LED} T_s} \right). \quad (9b)$$

Equation (9b) represents a general formula for determining the 365  
 scalability limit of a SIMO buck LED driver operating in DCM 366

and is referred to as a *scalable DCM-based SIMO scheme* for the sake of our ensuing discussion. In particular, when  $D_3 = 0$ , the SIMO buck LED driver operates in boundary conduction mode (BCM). Hence, (9a) and (9b) become (10a) and (10b), respectively. Also,  $N_{\max}$  in BCM is greater than or equal to that in DCM for the same set of design parameter values

$$N_{\max} = \frac{C_o \Delta v_{o \max}}{I_{\text{LED}} T_s} + 1 \quad (10a)$$

$$N_{\max} = \text{floor} \left( \frac{C_o \Delta v_{o \max}}{I_{\text{LED}} T_s} + 1 \right). \quad (10b)$$

For a single-output buck converter, the average inductor current is identical to the load current. Due to the nature of the time-multiplexing control scheme in the proposed SIMO converter, the average inductor current  $I_{L_{\text{avg}}}$  is the *sum* of the individual load current  $I_{\text{LED}}$  in each LED string. Assuming balanced load condition,  $I_{L_{\text{avg}}} = N \times I_{\text{LED}}$ , where  $N$  is the total number of LED strings. The average inductor current reaches its maximum value in BCM, resulting in a maximum transfer of power [16]. Since the current in each LED string remains the same, a theoretical upper bound of the total achievable number of LED strings in SIMO can be expressed as

$$N_{\max} = \frac{I_{L_{\text{avg-max}}}}{I_{\text{LED}}}. \quad (11)$$

By simple geometry,  $I_{L_{\text{avg-max}}}$  is given by the following equation [39]:

$$I_{L_{\text{avg-max}}} = \frac{m_1 D_1 T_s}{2} = \frac{(V_g - V_o) D_1 T_s}{2L}. \quad (12)$$

By substituting (12) into (11) and rearranging,  $T_s$  can be expressed as

$$T_s = \frac{2LN_{\max}I_{\text{LED}}}{D_1(V_g - V_o)}. \quad (13)$$

Now, by substituting (13) into (10a) and rearranging, we have

$$2LI_{\text{LED}}^2 N_{\max}^2 - 2LI_{\text{LED}}^2 N_{\max} - C_o \Delta v_{o \max} (V_g - V_o) D_1 = 0. \quad (14)$$

Equation (14) is a quadratic equation in  $N_{\max}$ . The discriminant  $\Delta$  of (14) can be expressed as

$$\Delta = 4L^2 I_{\text{LED}}^4 + 8LI_{\text{LED}}^2 C_o \Delta v_{o \max} (V_g - V_o) D_1 > 0. \quad (15)$$

Since  $(V_g - V_o) > 0$  for a buck switcher, the discriminant in (15) is always a positive number which implies that (14) has two real roots as given by

$$r_1, r_2 = \frac{2LI_{\text{LED}}^2 \pm \sqrt{\Delta}}{4LI_{\text{LED}}^2}. \quad (16)$$

Since  $N_{\max}$  must be a *positive integer*, the negative root is eliminated, leaving only the positive root, i.e.,

$$N_{\max\_BCM} = \text{floor} \left( \frac{1}{2} \times \left[ 1 + \sqrt{1 + \frac{2C_o \Delta v_{o \max} V_o (V_g - V_o)}{LI_{\text{LED}}^2 V_g}} \right] \right) \quad (17)$$

Equation (17) defines the theoretical maximum total number of outputs in SIMO operating in BCM. It is referred to as a

*scalable BCM-based SIMO scheme* which is a special case of *scalable DCM-based SIMO scheme*. In fact, it is observed that (11) is also valid for the case of DCM. By simple geometry, the switching period  $T_s$  in DCM can be expressed as

$$T_s = \frac{2LN_{\max}I_{\text{LED}}}{D_1(D_1 + D_2)(V_g - V_o)}. \quad (18)$$

Realizing that the same calculations that lead to (17) for the case of BCM can also be performed in DCM, the theoretical maximum total number of LED strings in a SIMO converter operating in DCM can, therefore, be written as<sup>1</sup>

$$N_{\max\_DCM} = \text{floor} \left( \frac{1}{2} \times (1 - D_3) \times \left[ 1 + \sqrt{1 + \frac{2C_o \Delta v_{o \max} (V_g - V_o) D_1}{LI_{\text{LED}}^2 (1 - D_3)}} \right] \right). \quad (19)$$

Notice that for the case of BCM,  $D_3 = 0$  and  $D_1 = V_o / V_g$ , (19) reduces to (17). Hence, (19) represents the generalized formula for the theoretical maximum total number of outputs in SIMO which is applicable to either BCM or DCM. It is also interesting to note that the average inductor current in DCM is smaller than (or equal to) that in BCM. As a result, for the same LED current, the theoretical maximum achievable number of outputs in SIMO operating in DCM is no greater than that in BCM, i.e.,  $N_{\max\_DCM} \leq N_{\max\_BCM}$ . In reality, the ESR of the output capacitor needs to be taken into consideration. Any current flowing through the output capacitor  $C_o$  must also flow through the  $R_{\text{ESR}}$ , resulting in an additional voltage drop of  $\Delta V_{\text{ESR}} = I_{\text{LED}} \times R_{\text{ESR}}$ . Hence,  $\Delta v_o$  can be expressed as

$$\Delta v_o = \Delta v_c + \Delta v_{\text{ESR}} = \Delta v_c + I_{\text{LED}} \times R_{\text{ESR}}. \quad (20)$$

Rearranging the terms in (20), we have

$$\Delta v_c = \Delta v_o - I_{\text{LED}} \times R_{\text{ESR}}. \quad (21)$$

Hence, (17) and (19) are modified slightly to become (22) and (23), respectively: BCM:

$$N_{\max\_BCM} = \text{floor} \left( \frac{1}{2} \times \left[ 1 + \sqrt{1 + \frac{2C_o V_o (\Delta v_{o \max} - I_{\text{LED}} R_{\text{ESR}}) (V_g - V_o)}{LI_{\text{LED}}^2 V_g}} \right] \right) \quad (22)$$

DCM:

$$N_{\max\_DCM} = \text{floor} \left( \frac{1}{2} \times (1 - D_3) \times \left[ 1 + \sqrt{1 + \frac{2C_o (\Delta v_{o \max} - I_{\text{LED}} R_{\text{ESR}}) (V_g - V_o) D_1}{LI_{\text{LED}}^2 (1 - D_3)}} \right] \right). \quad (23)$$

The presence of  $R_{\text{ESR}}$  in (22) and (23) reduces the theoretical maximum achievable number of outputs in SIMO. Therefore,

<sup>1</sup>In DCM,  $D_1$  can be expressed as:  $D_1 = M \sqrt{\frac{K}{1-M}}$ , where  $M = \frac{V_o}{V_g}$  and  $K = \frac{2L}{R_L T_s} = \frac{2LI_{\text{LED}}}{V_o T_s}$  [39].

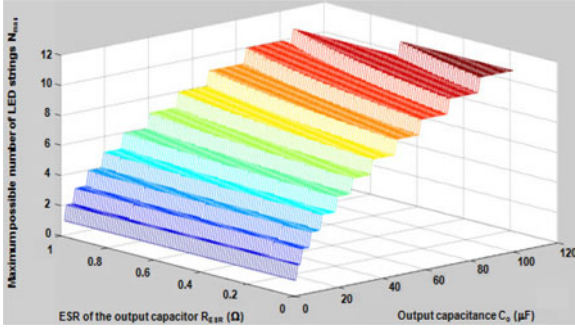


Fig. 10. Theoretical maximum achievable number of LED strings ( $N_{\max}$ ) versus the output capacitance ( $C_o$ ) and the capacitor ESR ( $R_{\text{ESR}}$ ) for the scalable BCM-based SIMO scheme.

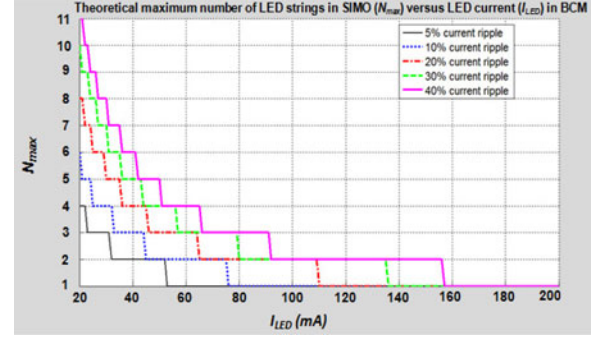


Fig. 11. Plot of theoretical maximum number of LED strings in SIMO ( $N_{\max}$ ) versus the LED current ( $I_{\text{LED}}$ ) in the scalable BCM-based SIMO scheme.

425 it is always recommended to choose an output capacitor with a  
426 smaller ESR, whenever possible. Fig. 10 shows the theoretical  
427 maximum total number of LED strings versus the output cap-  
428 acitance and capacitor ESR for the scalable BCM-based SIMO  
429 scheme, given a LED current of 80 mA and a maximum ripple  
430 current requirement of 40%<sub>P-P</sub>.

431 Intuitively, for a particular LED current, an increasing number  
432 of outputs can be achieved by using a larger output capacitor  
433 with the same ESR value. For instance, if the output capacitance  
434 is increased from 4.7 to 22  $\mu\text{F}$  (the ESR remains at 100 m $\Omega$ ),  
435 the theoretical model based on (22) suggests that the maximum  
436 total number of LED strings can be increased from three to six.  
437 It is also interesting to note that the maximum number of outputs  
438 in SIMO has a stronger dependence on the output capacitance  
439 than the capacitor ESR, as shown in Fig. 10.

440 On the other hand, it is useful to study how the LED current  
441 affects the maximum achievable number of outputs in SIMO.  
442 As an example, assuming balanced load and two LEDs con-  
443 nected in series per string, a scalable BCM-based SIMO scheme  
444 is investigated with these parameter values:  $L = 47 \mu\text{H}$ ,  $C_o =$   
445  $4.7 \mu\text{F}$ ,  $R_{\text{ESR}} = 100 \text{ m}\Omega$ ,  $V_g = 15 \text{ V}$ , and  $V_o = 6.4 \text{ V}$ . The  
446 relationship between  $N_{\max}$  and  $I_{\text{LED}}$  can be obtained by using  
447 (22) for different values of output voltage ripple  $\Delta v_{o\text{-max}}$ .  
448 Based upon the  $I$ - $V$  curve and/or SPICE model of the particular  
449 LED used, the corresponding output voltage ripple  $\Delta v_{o\text{-max}}$  can  
450 be determined from the LED current ripple requirement  $\Delta i_{\text{LED}}$ .  
451 The proposed design uses white LED [40] which is the target for  
452 LCD backlighting applications. For instance, a 20%<sub>P-P</sub> current  
453 ripple corresponds to around 2%<sub>P-P</sub> voltage ripple and a 40%<sub>P-P</sub>  
454 current ripple corresponds to around 4%<sub>P-P</sub> voltage ripple.  
455 Fig. 11 shows a plot of  $N_{\max}$  versus  $I_{\text{LED}}$  for  $\Delta i_{\text{LED}}$  rang-  
456 ing from 5%<sub>P-P</sub> to 40%<sub>P-P</sub>. This plot is beneficial to a practical  
457 SIMO design in two ways. First, for a given LED current and  
458 current ripple requirement, the theoretical maximum number  
459 of LED strings viable under the scalable BCM-based SIMO  
460 scheme can be extracted directly from the plot. Second, the

461 maximum LED current allowed in order for a SIMO to remain  
462 at the same scaling level can also be obtained from the plot. For  
463 instance, given a 20% current ripple requirement (i.e.,  $\Delta i_{\text{LED}} =$   
464  $20\%_{\text{P-P}}$ ), a SIMO (dual-string) configuration is possible as long  
465 as the LED current in each string is no more than 110 mA. In  
466 the event that an application demands an LED current greater  
467 than 110 mA, two options can be considered: 1) Relax the cur-  
468 rent ripple requirement whenever possible. A wider tolerance  
469 in  $\Delta i_{\text{LED}}$  is generally acceptable since the ripple frequency is  
470 too high for the human eye to detect. 2) Operate the SIMO buck  
471 LED driver in PCCM [17], [35], [36]. In PCCM, the floor of  
472 the inductor current is raised by a nonzero dc offset  $I_{\text{DC}}$  which  
473 distinguishes it from DCM. The proposed theoretical model can  
474 be extended to PCCM by adding a dc component to the aver-  
475 age inductor current. By going through similar calculations as  
476 in DCM, the theoretical maximum number of outputs in SIMO  
477 operating in PCCM is given by (24), as shown at the bottom of  
478 the page. It is interesting to note that (24) continues to apply to  
479 the cases of DCM and BCM. For instance, in DCM,  $I_{\text{DC}} = 0$   
480 and (24), therefore, reduces to (23).

481 In the event of unbalanced load with unequal current among  
482 the LED strings, the scalable DCM- or BCM-based SIMO  
483 scheme continues to hold. The only change is to replace  $I_{\text{LED}}$   
484 in (22) and (23) by  $\max(I_{\text{LED}})$ , where  $\max(I_{\text{LED}})$  denotes the  
485 largest LED current among all the LED strings. In other words,  
486 the maximum number of LED strings that can be realized in  
487 a SIMO buck LED driver is constrained by the largest LED  
488 current. Generally speaking, the input voltage  $V_g$ , output volt-  
489 age  $V_o$ , and the current ripple requirement are typically fixed  
490 parameters defined in the design specification. Without making  
491 any hardware changes (i.e.,  $L$  and  $C_o$  values are fixed), the pri-  
492 mary design variable in (22) and (23) is the LED current  $I_{\text{LED}}$ .  
493 In fact, the LED current is the dominant factor for determining  
494 the maximum possible number of outputs under the scalable  
495 DCM-/BCM-based SIMO scheme. By knowing the maximum  
496 LED current required for a particular application, the theoretical

$$N_{\max\_PCCM} = \text{floor} \left( \frac{1}{2I_{\text{LED}}} \times [(I_{\text{DC}} + (1 - D_3) I_{\text{LED}})] \times \left[ 1 + \sqrt{1 + \frac{2C_o(\Delta v_{o\text{-max}} - I_{\text{LED}} R_{\text{ESR}})(V_g - V_o) D_1(1 - D_3)}{L [I_{\text{DC}} - (1 - D_3) I_{\text{LED}}]^2}} \right] \right). \quad (24)$$

TABLE I  
DESIGN SPECIFICATION OF A SISO BUCK LED DRIVER IN DCM

Design Parameter	Value	Unit
Input Voltage ( $V_g$ )	15	V
Output Voltage ( $V_o$ )	6.32	V
LED Forward Current ( $I_{LED}$ )	80	mA
Switching Frequency ( $f_s$ )	100	kHz
Inductor ( $L$ )	47	$\mu$ H
Output Capacitor ( $C_o$ )	4.7	$\mu$ F
ESR of Output Capacitor ( $R_{ESR}$ )	100	m $\Omega$
Maximum LED Current Ripple ( $\Delta i_{LED}$ )	40	% <sub>p-p</sub>
Maximum Output Voltage Ripple ( $\Delta v_o$ )	4	% <sub>p-p</sub>
Duty Ratio of Idle Phase ( $D_3$ )	$\geq 10$	%

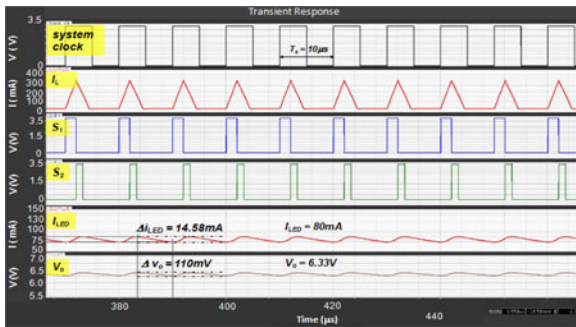


Fig. 12. Simulated steady-state waveforms for the SISO buck LED driver based on the design specification in Table I.

497 maximum achievable number of independently driven LED  
498 strings can be estimated in advance.

#### IV. SIMULATION RESULTS

500 Ideal macromodels based on the *scalable DCM-based SIMO*  
501 *scheme* were constructed and simulated in Cadence Spectre [27]  
502 in order to compare with the theoretical results in Section III. The  
503 design specification of a single-inductor single-output (SISO)  
504 buck converter is shown in Table I. The theoretical model based  
505 on (23) suggests that  $N_{max\_DCM} = 1$ , meaning only one LED  
506 string is viable. Fig. 12 shows the simulated steady-state wave-  
507 forms of the inductor current  $I_L$ , the LED currents  $I_{LED}$ , and  
508 the output voltages  $V_o$  of a SISO buck LED driver. The simu-  
509 lated steady-state LED current  $I_{LED}$  is approximately 80 mA  
510 which meets the design target. The simulated LED current ripple  
511  $\Delta i_{LED}$  is 18%<sub>p-p</sub> (also, the output voltage ripple  $\Delta v_o$  is  
512 1.7%<sub>p-p</sub>), which satisfies the maximum ripple requirement.  
513 Now, the SISO buck LED driver is transformed into SIDO  
514 by adding a second LED string. Fig. 13 shows the simulated  
515 steady-state waveforms from the resulting SIDO LED driver.

516 Despite the fact that the steady-state LED current in either  
517 string remains at 80 mA, the LED current ripple is more than  
518 40%<sub>p-p</sub> which violates the maximum ripple current require-  
519 ment. Hence, the simulation results show that SIDO is not viable  
520 based on the design requirement which is consistent with the  
521 theoretical result. By increasing the switching frequency from

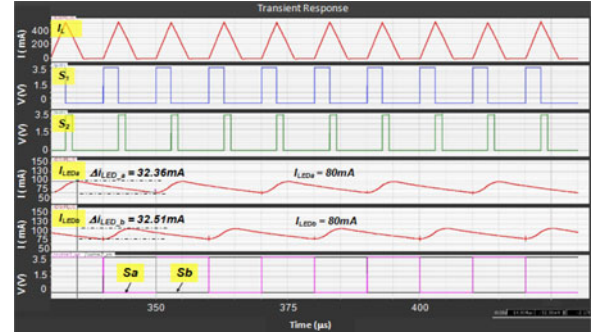


Fig. 13. Simulated steady-state waveforms showing SIDO is not viable since the 30%<sub>p-p</sub> maximum current ripple requirement is violated.

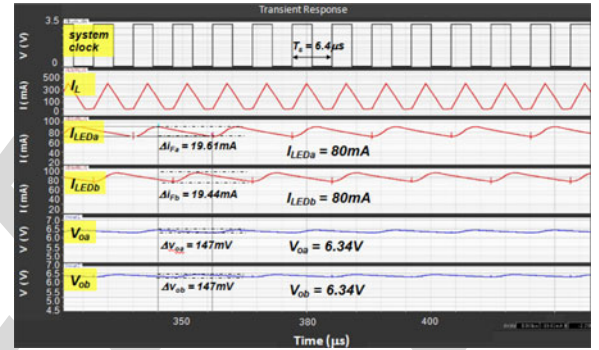


Fig. 14. Simulated steady-state waveforms showing SIDO is possible by increasing the switching frequency from 100 to 156.25 kHz.

100 to 156.25 kHz and keeping other parameters unchanged, 522  
 $N_{max\_DCM} = 2$  from (23). Fig. 14 shows the simulated wave- 523  
forms for the corresponding signals in a SIDO buck LED driver. 524  
The simulated LED current ripple  $\Delta i_{LED}$  is 24%<sub>p-p</sub> and the 525  
corresponding output voltage ripple  $\Delta v_o$  is 2.3%<sub>p-p</sub>, both of 526  
which satisfy their corresponding maximum ripple requirement. Con- 527  
sequently, both the theoretical and simulation results show that 528  
by increasing the switching frequency, a SIDO buck LED driver 529  
in DCM is feasible. 530

A third LED string is added to the SIDO buck LED driver to 531  
transform it into SIMO consisting of three independently driven 532  
LED strings. The LED current in each string remains unchanged 533  
at 80 mA as in the SISO or SIDO case. According to Fig. 11, 534  
the theoretical model suggests that for  $I_{LED} = 80$  mA, a *scal-* 535  
*able BCM-based SIMO* scheme with a maximum of *three* LED 536  
strings is feasible under the 40%<sub>p-p</sub> current ripple constraint. 537  
The switching period  $T_s$  is chosen to be 6  $\mu$ s using (13) which 538  
corresponds to a switching frequency of 166.67 kHz. Fig. 15 539  
shows the simulated waveforms from the resulting SIMO buck 540  
LED driver. The simulated LED current ripple  $\Delta i_{LED}$  is around 541  
35%<sub>p-p</sub> and the output voltage ripple  $\Delta v_o$  is 3.5%<sub>p-p</sub>, both of 542  
which satisfy their respective maximum ripple constraint. As a 543  
sanity check, the theoretical model based on (22) indeed sug- 544  
gests that a maximum possible number of *three* independen- 545  
tly driven LED strings can be achieved in the *scalable BCM-based* 546  
*SIMO* scheme. Hence, it is shown that the simulation result 547  
agrees with the corresponding theoretical result. On the other 548  
hand, it is important to examine the transient performance of the 549



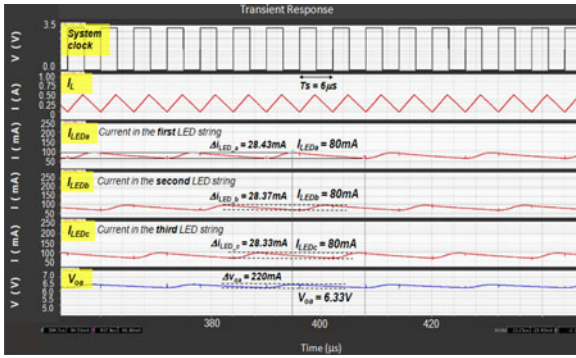


Fig. 15. Simulated steady-state waveforms of a three-string SIMO buck LED driver operating in BCM.

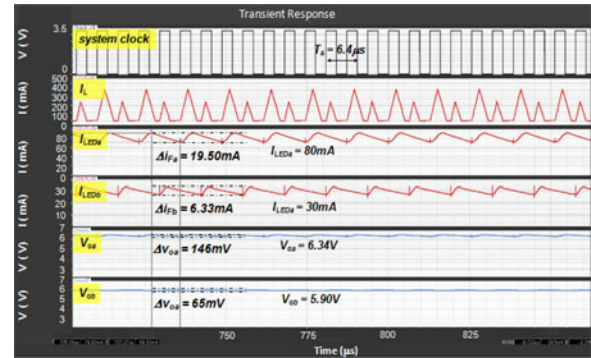


Fig. 17. Simulated steady-state waveforms of a SIDO buck LED driver with unbalanced load.

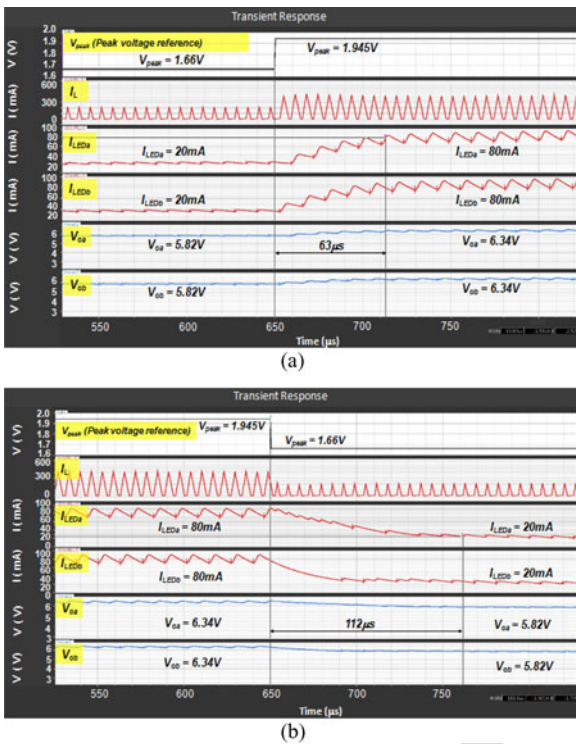


Fig. 16. Simulated transient waveforms for (a) peak reference step-up and (b) peak reference step-down response.

550 proposed SIDO buck LED driver. The LED current is changed  
 551 by adjusting the peak limit of the inductor current. By stepping  
 552 up the peak voltage reference ( $V_{peak}$  in Fig. 1) from 1.660 to  
 553 1.945 V in 400 ns, the peak inductor current limit is increased  
 554 by approximately 200 mA, leading to an increase in the nominal  
 555 LED current from 20 to 80 mA. The reference voltages  
 556 ( $V_{refa}$ ,  $V_{refb}$ ) are also stepped up from 100 to 340 mV in order  
 557 to maintain the same load current between the two LED strings.  
 558 Conversely, by stepping down  $V_{peak}$  from 1.945 to 1.660 V,  
 559 the LED current is reduced from 80 to 20 mA. Fig. 16 shows  
 560 the simulated transient behavior for the peak voltage reference  
 561 step-up and step-down response.

562 In the case of step-up reference response, the LED current in  
 563 either string settles to the steady-state nominal value of 80 mA  
 564 within 63  $\mu$ s. The output voltage reaches its target steady-state

value of 6.34 V. In the case of step-down reference response, 565  
 the LED current in either string settles to the steady-state nominal 566  
 value of 20 mA in less than 112  $\mu$ s. The output voltage 567  
 settles to its new steady-state value of 5.82 V without oscillations. 568  
 Hence, the simulation results show that the closed-loop 569  
 system remains in stable condition in response to a peak voltage 570  
 reference transient. 571

572 The effectiveness of the proposed SIDO converter to drive  
 573 unbalanced load is also investigated. As an example, the first  
 574 and second LED strings require an average current value of 80  
 575 and 30 mA, respectively. Unlike the balanced load case with  
 576 a constant peak inductor current limit, two distinct peak current  
 577 limits are employed for unbalanced load such that two  
 578 different average inductor (or load) current values can be gener-  
 579 ated in alternate clock cycles. Fig. 17 depicts the simulated  
 580 steady-state waveforms from the SIDO buck LED driver with  
 581 unbalanced load. The simulation results show that the first and  
 582 second LED strings are regulated with an average current value  
 583 of 80 and 30 mA, respectively. For the first string, the simu-  
 584 lated current ripple is 24.38%<sub>P-P</sub> and the output voltage ripple  
 585 is 2.3%<sub>P-P</sub>. Also, for the second string, the simulated current  
 586 ripple is 21.1%<sub>P-P</sub> and the output voltage ripple is 1.1%<sub>P-P</sub>.  
 587 Either string meets the maximum ripple requirements. The simu-  
 588 lation results demonstrate that the proposed SIDO converter is  
 589 capable of delivering unequal currents to the two LED strings  
 590 simultaneously.

## 591 V. EXPERIMENTAL RESULTS

592 The proposed SIDO buck LED driver was implemented on  
 593 a field-programmable gate array (FPGA)-based hardware proto-  
 594 type in accordance with the design specification provided in  
 595 Table I. The switching frequency is increased to 156.25 kHz in  
 596 order to satisfy the LED current ripple requirement. A photo of  
 597 the experimental setup is shown in Fig. 18. The power stage of  
 598 the buck converter consists of discrete ICs from International  
 599 Rectifier such as power MOSFETs (IRF7828), dual-channel  
 600 gate driver (IR2110), and output switches (IRF9388), as well as  
 601 surface-mount inductor and low-ESR capacitors. In actual im-  
 602 plementation, the top level of the proposed digital controller is  
 603 partitioned into two major functional blocks. The functionality  
 604 of the first block is to control the switching action of the power

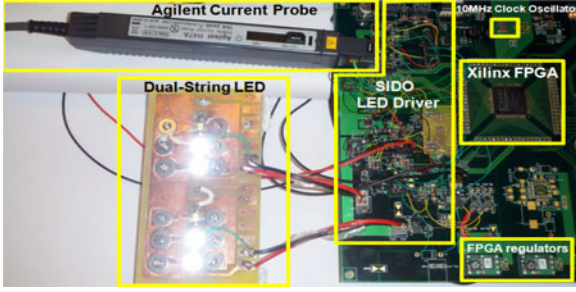


Fig. 18. Experimental setup for the proposed SIDO buck LED driver.

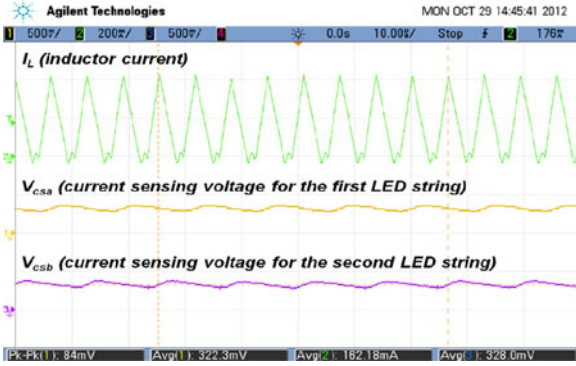


Fig. 19. Measured waveforms for inductor current and current sense feedback voltage.

605 stage by detecting the peak-crossing and zero-crossing events of the inductor current. It was implemented in hierarchical gate-level schematics using primitives and macros available from the Xilinx Spartan-3 Generation library. Dead-time logic is included to prevent shoot-through current of the power switches. The second logical block is used to control the switching sequence of the two output switches by continuously monitoring the current-sense feedback signals. It was modeled as an FSM in Verilog RTL. Only one of the two output switches can be ON and the other must be OFF per switching cycle. Dead-time logic is also added to prevent cross conduction between outputs. The two logical blocks are synchronized by the system clock to ensure that the high-side power switch and the output switches are triggered from the same clock edge. The entire digital controller was implemented with Xilinx Spartan-3E (XC3S250E) FPGA. The quasi-hysteretic control logic was realized using 4-ns fast comparators (AD8611 from Analog Devices) and semicustom synchronous logic.

623 Using a current sensing resistor of  $4\ \Omega$  and reference voltage of  $320\ \text{mV}$ , the target current in each of the two LED strings is  $80\ \text{mA}$ . Fig. 19 shows the current sensing feedback voltage ( $V_{CSA}$ ,  $V_{CSB}$ ) from which the corresponding average load current can be obtained, i.e.,  $I_{LED} = V_{CS}/R_{CS}$ . The average inductor current is measured to be  $162\ \text{mA}$ , which is the sum of the load currents in both LED strings. The average current values in the first and second LED string are measured to be around  $80.6$  and  $82\ \text{mA}$ , respectively. The measured LED current ripple  $\Delta I_{LED}$  in either string is around  $26\%_{P-P}$ , which is reasonably close to the simulated current ripple of  $24\%_{P-P}$ . In addition, the nominal output voltages in the first and second string are

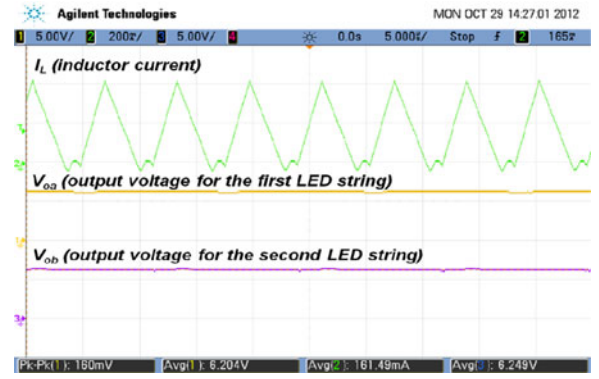
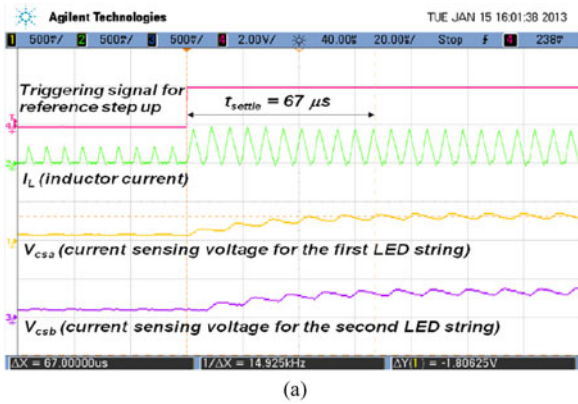


Fig. 20. Measured waveforms for inductor current and output voltage in either LED string.

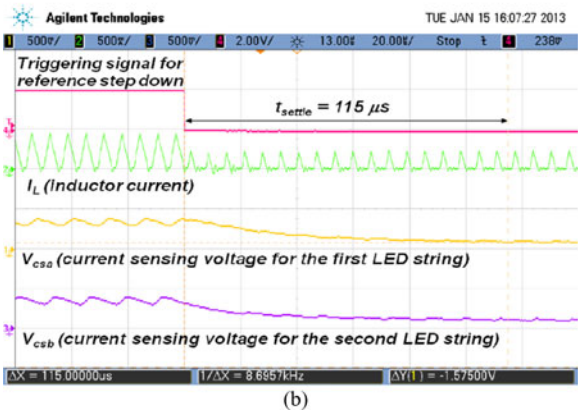
635 measured to be  $6.204$  and  $6.249\ \text{V}$ , respectively, as shown in 636  
 637 Fig. 20. Under this balanced load condition, the measured current and voltage values are in close agreement between the two LED strings. The output voltage ripple is also measured to be around  $2.57\%_{P-P}$ , compared to  $2.3\%_{P-P}$  from simulation. Therefore, the experimental results are shown to be consistent with the corresponding simulation ones. On the other hand, the measured power conversion efficiency of the proposed SIDO converter is  $80\%$  which is comparable to conventional driving topologies [41]. The efficiency can be further increased by employing a current-sensing resistor with a smaller value.

642 The transient response of the proposed SIDO buck LED driver is verified experimentally by measuring its peak voltage reference step response. An 8-bit digital-to-analog converter (AD558 from Analog Devices) is used to enable programming of the peak voltage reference  $V_{PEAK}$  and the current-sense voltage references ( $V_{REFA}$ ,  $V_{REFB}$ ) by the Xilinx FPGA. The measured waveforms of the inductor current and the voltage at the current sensing nodes in response to a peak voltage reference step are shown in Fig. 21. The settling time of the transient response is also measured and compared with the simulated settling time. For the step-up response, it is observed that the current-sensing voltage  $V_{CSA}$  in the first LED string steps up from  $81.8$  to  $325.4\ \text{mV}$ , which corresponds to an increase in the average load current from  $20.5$  to  $81.3\ \text{mA}$ . Similarly, the current-sensing voltage  $V_{CSB}$  in the second LED string steps up from  $94.1$  to  $327.6\ \text{mV}$ , which corresponds to an increase in the average load current from  $23.5$  to  $81.9\ \text{mA}$ . The settling time for the step-up response is measured to be  $67\ \mu\text{s}$ , compared to  $63\ \mu\text{s}$  from simulation. The measured results for the step-down response are the reverse of those from the step-up response. The only difference is that it takes longer for the step-down transient to settle. The settling time for the step-down response is measured to be  $115\ \mu\text{s}$ , compared to  $112\ \mu\text{s}$  from simulation. The measured settling times are shown to be very close to the simulated ones. The experimental results confirm that the system remains in stable condition when it is perturbed by the peak voltage reference transient.

673 The unbalanced load scenario in the proposed SIDO buck LED driver is also verified experimentally. The measured average load current values in the first and second LED string are 674 675



(a)



(b)

Fig. 21. Measured transient waveforms in response to (a) peak reference step-up and (b) peak reference step-down.

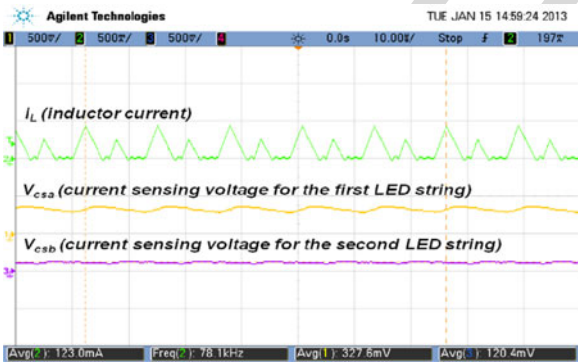


Fig. 22. Measured waveforms for inductor current and current sense voltages.

676 around 81.9 and 30.1 mA, respectively. Fig. 22 shows the measured  
 677 waveforms for the inductor current and the current-sensing  
 678 voltage per string. The inductor current waveform indicates that  
 679 the proposed driver operates in DCM with *two* distinct peak  
 680 current limits. Fig. 23 shows the measured inductor current and  
 681 the output voltage in either string. The measured output voltage  
 682 values in the first and second LED string are 6.22 and 5.70 V,  
 683 respectively. The experimental results demonstrate that the proposed  
 684 driver is capable of driving two independent LED strings  
 685 concurrently with different load current.

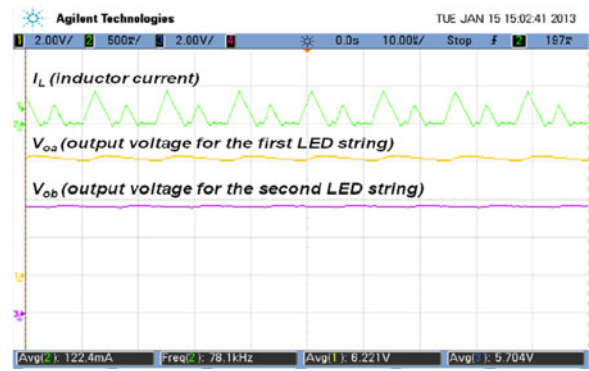


Fig. 23. Measured waveforms for inductor current and output voltages.

## VI. CONCLUSION

686 The proposed SIDO buck LED driver was implemented in  
 687 FPGA-based hardware. The experimental results correlate well  
 688 with simulation ones. The scalability of the proposed SIDO buck  
 689 LED driver to SIMO is closely examined. A general formula  
 690 for determining the theoretical maximum achievable number of  
 691 LED strings in SIMO is derived. The simulation results were  
 692 shown to be consistent with those obtained from the theoretical  
 693 model for the same design parameter values. The quasi-  
 694 hysteretic digital control scheme does not require loop compen-  
 695 sation which simplifies the control loop design and reduces  
 696 component count. In addition, the proposed SIMO architecture  
 697 offers the advantage of driving a larger number of parallel LED  
 698 strings without being limited by the maximum current rating of  
 699 the LED. It also enables dimming for the LED strings without  
 700 additional dimming transistors. Local bus voltage and current  
 701 optimization in each individual LED string compensates for the  
 702 variability of the LED's forward voltage, which reduces power  
 703 loss and enables mixing of white LEDs from different bins to  
 704 lower LED costs.  
 705

## REFERENCES

- [1] C.-Y. Hsieh, C.-Y. Yang, and K.-H. Chen, "A charge-recycling buck-store and boost-restore (BSBR) technique with dual outputs for RGB LED backlight and flashlight module," *IEEE Trans. Power Electron.*, vol. 24, no. 8, pp. 1914–1925, Aug. 2009.
- [2] S.-Y. Lee, J.-W. Kwon, H.-S. Kim, M.-S. Choi, and K.-S. Byun, "New design and application of high efficiency LED driving system for RGB-LED backlight in LCD display," in *Proc. 37th IEEE Power Electron. Spec. Conf.*, 2006, pp. 1–5.
- [3] H.-J. Chiu, Y.-K. Lo, J.-T. Chen, S.-J. Cheng, C.-Y. Lin, and S.-C. Mou, "A high-efficiency dimmable led driver for low-power lighting applications," *IEEE Trans. Ind. Electron.*, vol. 57, no. 2, pp. 735–743, Feb. 2010.
- [4] C.-H. Liu, C.-Y. Hsieh, Y.-C. Hsieh, T.-J. Tai, and K.-H. Chen, "SAR-Controlled adaptive off-time technique without sensing resistor for achieving high efficiency and accuracy led lighting system," *IEEE Trans. Circuits Syst. I, Reg. Papers*, vol. 57, no. 6, pp. 1384–1394, Jun. 2010.
- [5] C.-H. Wu and C.-L. Chen, "High-efficiency current-regulated charge pump for a white LED driver," *IEEE Trans. Circuits Syst. II, Exp. Briefs*, vol. 56, no. 10, pp. 614–618, Oct. 2009.
- [6] P. Malcovati, M. Belloni, F. Gozzini, C. Bazzani, and A. Baschiroto, "A 0.18μm CMOS 91%-efficiency 0.1-to-2 A scalable buck-boost DC-DC converter for LED drivers," in *Proc. ISSCC Dig. Tech. Papers*, Feb. 2012, pp. 280–281.
- [7] S. Rao, Q. Khan, S. Bang, D. Swank, A. Rao, W. McIntyre, and P. K. Hanumolu, "A 1.2 A buck-boost LED driver with 13% efficiency

- improvement using error-averaged SenseFET-Based current sensing," in *Proc. ISSCC Dig. Tech. Papers*, Feb. 2011, pp. 238–239.
- [8] S.-I. Hong, J.-W. Han, D.-H. Kim, and O.-K. Kwon, "A double-loop control LED backlight driver IC for medium-sized LEDs," in *Proc. ISSCC Dig. Tech. Papers*, Feb. 2010, pp. 116–117.
- [9] M.-H. Huang and K.-H. Chen, "Single-inductor multi-output (SIMO) DC-DC converters with high light-load efficiency and minimized cross-regulation for portable devices," *IEEE J. Solid-State Circuits*, vol. 44, no. 4, pp. 1099–1111, Apr. 2009.
- [10] E. Bonizzoni, F. Borghetti, P. Malcovati, F. Maloberti, and B. Niessen, "A 200 mA 93% peak efficiency single-inductor dual-output DC-DC buck converter," in *Proc. IEEE ISSCC Dig. Tech. Papers*, Feb. 2007, pp. 526–619.
- [11] C.-Y. Hsieh and K.-H. Chen, "Boost DC-DC converter with fast reference tracking (FRT) and charge-recycling (CR) techniques for high-efficiency and low-cost LED driver," *IEEE J. Solid-State Circuits*, vol. 44, no. 9, pp. 2568–2580, Sep. 2009.
- [12] H. Chen, Y. Zhang, and D. Ma, "A SIMO parallel-string driver IC for dimmable LED backlighting with local bus voltage optimization and single time-shared regulation loop," *IEEE Trans. Power Electron.*, vol. 27, no. 1, pp. 452–462, Jan. 2012.
- [13] D. Ma, W.-H. Ki, P. K. T. Mok, and C.-Y. Tsui, "Single-inductor multiple-output switching converters with bipolar outputs," in *Proc. IEEE Int. Symp. Circuits Syst.*, May 2001, vol. 3, pp. 301–304.
- [14] D. Ma, W.-H. Ki, C.-Y. Tsui, and P. K. T. Mok, "A 1.8 V single-inductor dual-output switching converter for power reduction techniques," in *Proc. IEEE Symp. VLSI Circuits*, Jun. 2001, pp. 137–140.
- [15] W.-H. Ki and D. Ma, "Single-inductor multiple-output switching converters," in *Proc. 32nd IEEE Power Electron. Spec. Conf.*, Jun. 2001, vol. 1, pp. 226–231.
- [16] D. Ma, W.-H. Ki, C.-Y. Tsui, and P. K. T. Mok, "Single-inductor multiple-output switching converters with time-multiplexing control in discontinuous conduction mode," *IEEE J. Solid-State Circuits*, vol. 38, no. 1, pp. 89–100, Jan. 2003.
- [17] D. Ma, W.-H. Ki, and C.-Y. Tsui, "A pseudo-CCM/DCM SIMO switching converter with freewheel switching," *IEEE J. Solid-State Circuits*, vol. 38, no. 6, pp. 1007–1014, Jun. 2003.
- [18] D. Kwon and G. A. Rincón-Mora, "Single-inductor multiple-output switching DC-DC converters," *IEEE Trans. Circuits Syst. II, Exp. Briefs*, vol. 56, no. 8, pp. 614–618, Aug. 2009.
- [19] K.-S. Seol, Y.-J. Woo, G.-H. Cho, G.-H. Cho, and J.-W. Lee, "A synchronous multioutput step-up/down DC-DC converter with return current control," *IEEE Trans. Circuits Syst. II, Exp. Briefs*, vol. 56, no. 3, pp. 210–214, Mar. 2009.
- [20] C.-W. Leng, C.-H. Yang, and C.-H. Tsai, "Digital PWM controller for SIDO switching converter with time-multiplexing scheme," in *Proc. Int. Symp. VLSI Design Autom. Test*, Apr. 2009, pp. 52–55.
- [21] Y.-J. Moon, Y.-S. Roh, J.-C. Gong, and C. Yoo, "Load-independent current control technique of a single-inductor multiple-output switching DC-DC converter," *IEEE Trans. Circuits Syst. II, Exp. Briefs*, vol. 59, no. 1, pp. 50–54, Jan. 2012.
- [22] F. Su, W.-H. Ki, and C.-Y. Tsui, "Ultra fast fixed-frequency hysteretic buck converter with maximum charging current control and adaptive for DVS applications," *IEEE J. Solid-State Circuits*, vol. 43, no. 4, pp. 815–822, Apr. 2008.
- [23] W.-H. Ki, K.-M. Lai, and C. Zhan, "Charge balance analysis and state transition analysis of hysteretic voltage mode switching converters," *IEEE Trans. Circuits Syst. I, Reg. Papers*, vol. 58, no. 5, pp. 1142–1153, May 2011.
- [24] K. K.-S. Leung and H. S.-H. Chung, "Dynamic hysteresis band control of the buck converter with fast transient response," *IEEE Trans. Circuits Syst. II, Exp. Briefs*, vol. 52, no. 7, pp. 398–402, Jul. 2005.
- [25] H. Eachempatti, S. Ganta, J. Silva-Martinez, and H. Martínez-García, "SIDO buck converter with independent outputs," in *Proc. 53rd IEEE Int. Midwest Symp. Circuits Syst.*, Aug. 2010, pp. 37–40.
- [26] F. Su and W.-H. Ki, "Digitally assisted quasi- $V^2$  hysteretic buck converter with fixed frequency and without using Large-ESR capacitor," in *Proc. ISSCC Dig. Tech. Papers*, Feb. 2009, pp. 446–447.
- [27] Cadence Spectre Circuit Simulator Datasheet [Online]. Available: [http://www.cadence.com/products/cic/spectre\\_circuit/pages/default.aspx](http://www.cadence.com/products/cic/spectre_circuit/pages/default.aspx)
- [28] M. Doshi and R. Zane, "Digital architecture for driving large LED arrays with dynamic bus voltage regulation and phase shifted PWM," in *Proc. Appl. Power Electron. Conf.*, Feb. 2007, pp. 287–293.
- [29] W.-S. Oh, D. Cho, K.-M. Cho, G.-W. Moon, B. Yang, and T. Jang, "A novel two-dimensional adaptive dimming technique of X-Y channel drivers for LED backlight system in LCD TVs," *J. Display Technol.*, vol. 5, no. 1, pp. 20–26, Jan. 2009.
- [30] Datasheet: LP8545, "LP8545 High-efficiency LED backlight driver for notebooks," Texas Instruments Incorporated, [Online] Available: <http://www.ti.com/general/docs/lit/getliterature.tsp?genericPartNumber=lp8545&fileType=pdf>
- [31] Datasheet: MAX16814, "Integrated, 4-channel, high-brightness LED driver with high-voltage DC-DC controller," Maxim Integrated Products, Inc., [Online], Available: <http://datasheets.maximintegrated.com/en/ds/MAX16814.pdf>
- [32] K. H. Loo, W. K. Lun, S. C. Tan, Y. M. Lai, and C. K. Tse, "On driving techniques for LEDs: Toward a generalized methodology," *IEEE Trans. Power Electron.*, vol. 24, no. 12, pp. 2967–2976, Dec. 2009.
- [33] W. K. Lun, K. H. Loo, S. C. Tan, Y. M. Lai, and C. K. Tse, "Bilevel current driving technique for LEDs," *IEEE Trans. Power Electron.*, vol. 24, no. 12, pp. 2920–2932, Dec. 2009.
- [34] S. C. Tan, "General n-level driving approach for improving electrical-to-optical energy-conversion efficiency of fast-response saturable lighting devices," *IEEE Trans. Ind. Electron.*, vol. 57, no. 4, pp. 1342–1353, Apr. 2010.
- [35] D. Ma and W.-H. Ki, "Fast transient PCCM switching converter with freewheel switching control," *IEEE Trans. Circuits Syst. II, Exp. Briefs*, vol. 54, no. 9, pp. 825–829, Sep. 2007.
- [36] D. Ma, W.-H. Ki, and C.-Y. Tsui, "Single-inductor multiple-output switching converters in PCCM with freewheel switching," U.S. Patent 7 432 614, Oct. 7, 2008.
- [37] Application Note: AN-1656, "Design challenges of switching LED drivers," Texas Instruments Incorporated, [Online] Available: <http://www.ti.com/general/docs/lit/getliterature.tsp?literatureNumber=snva253&fileType=pdf>
- [38] Solutions Guide, "LED drivers for high-brightness lighting," Texas Instruments Incorporated, [Online], Available: <http://www.ti.com/general/docs/lit/getliterature.tsp?baseLiteratureNumber=snvy001>
- [39] R. W. Erickson and D. Maksimovic, *Fundamentals of Power Electronics*, 2nd ed. New York, NY, USA: Springer, 2001.
- [40] Datasheet: SMD5730, "SMD 5730 White LED Datasheet," APT Electronics Ltd., [Online], Available: <http://www.appt-hk.com/en/product/?95.html>
- [41] Z. Ye, F. Greenfeld, and Z. Liang, "Design considerations of a high power factor SEPIC converter for high brightness white LED lighting applications," in *Proc. IEEE Power Electron. Spec. Conf.*, 2008, pp. 2657–2663.



**Albert T. L. Lee** received the Bachelor of Science degree in electrical engineering from the University of Wisconsin, Madison, USA, in 1994, and the Master of Science degree from the University of Michigan, Ann Arbor, USA, in 1996. He is currently working toward the Doctor of Philosophy degree in electronic and computer engineering at the Hong Kong University of Science and Technology, Kowloon, Hong Kong.

He joined Intel Corporation, Hillsboro, OR, USA, in 1996 as a Senior Component Design Engineer and was involved in the development of Intel's P6 family microprocessors. In 2001, he served as a Senior Corporate Application Engineer in the System-Level Design Group at Synopsys Inc., Mountain View, CA, USA. In 2003, he joined the Hong Kong Applied Science and Technology Research Institute Company Ltd. and served as EDA Manager in the Wireline Communications Group. In 2006, he joined the Giant Electronics Limited as Hardware Design Manager and became Associate General Manager in 2008. His research interests include mixed-signal system-level design, LED driver, power management system, and very large scale integration circuits.

867  
868  
869  
870  
871  
872  
873  
874  
875  
876  
877  
878  
879  
880  
881  
882  
883  
884  
885  
886  
887  
888  
889  
890



**Johnny K. O. Sin** (S'79–M'88–SM'96–F'12) received the B.A.Sc., M.A.Sc., and Ph.D. degrees in electrical engineering from the University of Toronto, Toronto, ON, Canada, in 1981, 1983, and 1988, respectively.

From 1988 to 1991, he was a Senior Member of the research staff of Philips Laboratories, Briarcliff Manor, NY, USA. In August 1991, he joined the Department of Electronic and Computer Engineering, The Hong Kong University of Science and Technology, Kowloon, Hong Kong, where he has been a Full

Professor since 2001. He is the holder of 13 patents, and the author of more than 270 papers in technical journals and refereed conference proceedings. His research interests include microelectronic and nanoelectronic devices and fabrication technology, particularly novel power semiconductor devices and ICs, and system-on-a-chip applications using CMOS and power transistors and silicon-embedded magnetic and capacitive devices.

Dr. Sin was an Editor for the IEEE ELECTRON DEVICES LETTERS from 1998 to 2010. He is a member of the Power Devices and IC's Technical Committee of the IEEE Electron Devices Society. He is also a Technical Committee member of the International Symposium on Power Semiconductor Devices and IC's. He is a Fellow of the IEEE for contributions to the design and commercialization of power semiconductor devices.



**Philip C. H. Chan** (SM'97–F'07) received the Bachelor of Science degree in electrical engineering from the University of California at Davis, Davis, USA, in 1973, and the Master of Science and Doctor of Philosophy degrees in electrical engineering from the University of Illinois at Urbana-Champaign, Urbana, USA, in 1975 and 1978, respectively.

He later joined Intel Corporation, Santa Clara, CA, USA, in 1981 and became a Senior Project Manager in Technology Development. He joined the Hong Kong University of Science and Technology

(HKUST) in 1991 as a founding member. He served at HKUST as the Associate Dean of Engineering and Head of the Department of Electronic and Computer Engineering. He became the Dean of Engineering in September 2003. He joined the Hong Kong Polytechnic University, Hong Kong, in 2010 as the Deputy President and Provost. His research interests include very large scale integration devices, circuits, electronic packaging, and integrated sensors.

Dr. Chan received the ECE Distinguished Alumni Award from the University of Illinois, Urbana-Champaign in 2010.

891  
892  
893  
894  
895  
896  
897  
898  
899  
900  
901  
902  
903  
904  
905  
906  
907  
908  
909  
910

IEEE  
Proof

912 Q1. Author: Please provide year information in Refs. [27], [30], [31], [37], [38], and [40].

IEEE  
Proof

# Scalability of Quasi-Hysteretic FSM-Based Digitally Controlled Single-Inductor Dual-String Buck LED Driver to Multiple Strings

Albert T. L. Lee, Johnny K. O. Sin, *Fellow, IEEE*, and Philip C. H. Chan, *Fellow, IEEE*

**Abstract**—There has been growing interest in single-inductor multiple-output (SIMO) dc–dc converters due to its reduced cost and smaller form factor in comparison with using multiple single-output converters. An application for such a SIMO-based switching converter is to drive multiple LED strings in a multichannel LED display. This paper proposes a quasi-hysteretic finite-state-machine-based digitally controlled single-inductor dual-output buck switching LED driver operating in discontinuous conduction mode (DCM) and extends it to drive multiple outputs. Based on the time-multiplexing control scheme in DCM, a theoretical upper limit of the total number of outputs in a SIMO buck switching LED driver for various backlight LED current values can be derived analytically. The advantages of the proposed SIMO LED driver include reducing the controller design complexity by eliminating loop compensation, driving more LED strings without limited by the maximum LED current rating, performing digital dimming with no additional switches required, and optimization of local bus voltage to compensate for variability of LED forward voltage  $V_F$  in each individual LED string with smaller power loss. Loosely binned LEDs with larger  $V_F$  variation can, therefore, be used for reduced LED costs.

**Index Terms**—Boundary conduction mode (BCM), discontinuous conduction mode (DCM), finite-state machine (FSM), single-inductor dual-output (SIDO), single-inductor multiple-output (SIMO).

## I. INTRODUCTION

A LED driver is essentially a current source (or sink) which maintains a constant current required for achieving the desired color and luminous flux from an array of LEDs. A number of highly efficient switching LED drivers have been reported in the literature and their primary objective is to achieve high power conversion efficiency [1]–[11]. Besides efficiency, another important consideration is the scalability of the existing single-inductor dual-output (SIDO) switching converter to drive multiple independent LED strings in a single-inductor multiple-output (SIMO) topology for reduced cost and smaller

form factor [12]. However, in practice, only a finite number of outputs can be served by each LED driver.

The prior arts of SIMO switching converter use either one of two ways to distribute energy from a single power supply to multiple outputs with a single inductor, namely multiple energizing phases [13]–[20] and single energizing phase per switching cycle [21]. The former with time-multiplexing control leads to much better suppression of cross regulation because the outputs are decoupled in time. In this paper, a quasi-hysteretic finite-state machine (FSM)-based digital control scheme is employed in a SIDO buck LED driver consisting of two independent parallel strings operating in discontinuous conduction mode (DCM). The extension of this SIDO architecture to SIMO is formally investigated. The proposed SIMO-based switching buck LED driver enables separate control of the three primary colors (red, green, and blue), thereby offering more flexibility for color mixing. The rest of this paper is organized as follows. Section II introduces the proposed quasi-hysteretic FSM-based digital controller for a SIDO switching buck LED driver operating in DCM. Section III provides a theoretical analysis on the scalability of the proposed digital control scheme from SIDO to SIMO and suggests a general formula for determining the theoretical upper bound in the total number of outputs in SIMO. Section IV shows Cadence Spectre simulation results that are used to verify the theoretical model. Section V contains the experimental results for the proposed digitally controlled SIDO buck LED driver. Section VI concludes our research effort.

## II. QUASI-HYSTERETIC FSM-BASED DIGITAL CONTROL FOR SIDO LED DRIVER

A SIDO switching converter with time-multiplexing control scheme operating in DCM was first reported in [13]–[16]. With such kind of time-multiplexing control scheme, a SIDO converter can easily be extended to drive multiple outputs and it exhibits negligible cross regulation in DCM. A SIMO parallel-string LED driver operating in DCM has recently been reported [12]. It uses an analog-based controller with dominant pole compensation for stability, and time-multiplexing control in DCM is employed to suppress cross regulation among the LED strings. Unlike conventional pulse width modulation (PWM)-based analog controllers, the proposed digital controller utilizing quasi-hysteretic control does not require any compensation circuits because of its inherent stability [22]–[24], hence simplifying the control loop design and reducing the component count and cost. Quasi-hysteretic control offers a good

Manuscript received November 7, 2012; revised January 22, 2013; accepted March 11, 2013. Recommended for publication by Associate Prof. J. M. Alonso.

A. T. L. Lee and J. K. O. Sin are with the Department of Electronic and Computer Engineering, The Hong Kong University of Science and Technology, Kowloon, Hong Kong (e-mail: alee@ust.hk; eesin@ust.hk).

P. C. H. Chan is with Hong Kong Polytechnic University, Hong Kong (e-mail: Philip.Chan@inet.polyu.edu.hk).

Color versions of one or more of the figures in this paper are available online at <http://ieeexplore.ieee.org>.

Digital Object Identifier 10.1109/TPEL.2013.2253804

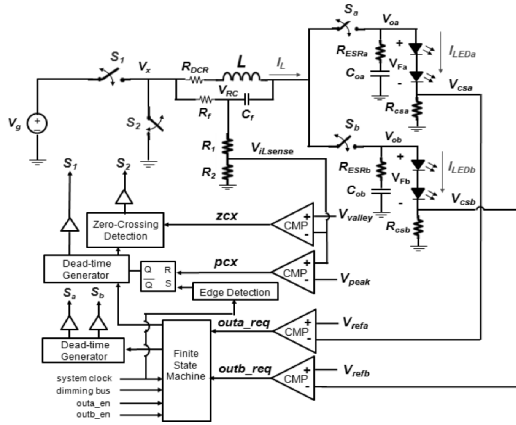


Fig. 1. System architecture of the quasi-hysteretic FSM-based digitally controlled SIDO buck LED driver.

85 compromise between traditional fixed-frequency PWM control  
 86 and pure hysteretic control with variable switching frequency.  
 87 In the proposed design, an external clock is used to synchron-  
 88 ize the buck LED driver which switches at a fixed frequency.  
 89 Fast comparators are used to control the on-time of the high-  
 90 side and low-side power switches by monitoring the inductor  
 91 current. This is particularly suitable for lighting applications  
 92 where variable switching frequencies are not desirable. The re-  
 93 configurable and scalability of a digital controller makes it  
 94 especially attractive for SIMO.

95 A major drawback of the previously proposed SIMO LED  
 96 driver operating in DCM [12] is that since the LED current is  
 97 discontinuous, the LED endures a higher maximum peak current  
 98 for the same average current required. In other words, the LED  
 99 could potentially be operating close to its absolute maximum  
 100 current rating, thereby increasing the current stress and possibly  
 101 shortening the operating lifetime of the LED. In their approach,  
 102 the LED current scales with the number of LED strings in SIMO.  
 103 Hence, the maximum current rating of the LED unnecessarily  
 104 restricts the maximum achievable number of LED strings which  
 105 can be implemented in SIMO. In the proposed design, the LED  
 106 current is always continuous and the LED can be regulated very  
 107 close to the target average current value which is much lower  
 108 than its maximum current rating. During the time interval when  
 109 the output switch is OFF, the output capacitor, acting as a con-  
 110 stant current source, continues to discharge its current to the  
 111 corresponding LED string. When the output switch is ON, the  
 112 power stage is reconnected to the LED string and the induc-  
 113 tor current is transferred to the output capacitor and the LED  
 114 string simultaneously. The current-sense feedback control en-  
 115 sures that the LED current is maintained at the desired dc level.  
 116 Hence, a time-continuous current is supplied to the LED string.  
 117 Consequently, the LED current does *not* scale with the number  
 118 of LED strings in the proposed SIMO architecture, making it  
 119 possible to drive more LED strings without inducing too much  
 120 stress on the LEDs. Fig. 1 shows the system architecture of the  
 121 proposed quasi-hysteretic FSM-based digitally controlled SIDO  
 122 buck switching LED driver which takes into account the parasitic  
 123 effects including the dc resistance (DCR) of the inductor  $L$

and equivalent series resistance (ESR) of the output capacitors  
 124 ( $C_{oa}, C_{ob}$ ). The two independently driven LED strings share  
 125 the same inductor  $L$  and the two main power switches ( $S_1, S_2$ )  
 126 of the buck converter. The output switches ( $S_a, S_b$ ) enable the  
 127 charge stored in the inductor to be distributed between the two  
 128 outputs in a time-multiplexed fashion. Dead-time generators  
 129 are used to eliminate shoot-through current by ensuring that  
 130  $S_1$  and  $S_2$  are not turned ON simultaneously. Dead-times are  
 131 also introduced between  $S_a$  and  $S_b$  to prevent inadvertent cross  
 132 conduction between the two LED strings.  
 133

Since an LED is essentially a current driven device, an LED  
 134 driver typically regulates the LED current rather than its forward  
 135 voltage. A straightforward way is to insert a small high-precision  
 136 current sensing resistor ( $R_{csa}, R_{csb}$ ) in series with the corre-  
 137 sponding LED string to sense the LED current by converting it  
 138 to the current-sense voltage ( $V_{csa}, V_{csb}$ ). The current-sense vol-  
 139 tage is then compared with the reference voltage ( $V_{refa}, V_{refb}$ )  
 140 to generate the corresponding logic signals ( $outa\_req, outb\_req$ )  
 141 which determine the opening or closing of the two output  
 142 switches in a SIDO buck converter. Since the LED's  $I-V$  curve  
 143 is usually provided by the LED manufacturer, the target dc cur-  
 144 rent value for a particular LED string can be set by choosing  
 145 an appropriate reference voltage. On the other hand, a two-limit  
 146 hysteretic control determines the on-time of the high-side and  
 147 low-side power switches ( $S_1, S_2$ ) of the buck converter. The  
 148 upper and lower limits of the inductor current, namely the peak  
 149 current limit and the valley current limit, define the average  
 150 value of the inductor current which is the *total* LED current for  
 151 a SIDO buck LED driver. In DCM, the valley current limit is  
 152 set to zero to prevent the inductor current from going negative  
 153 which degrades the power conversion efficiency [12], [16], [25].  
 154 As illustrated in Fig. 1,  $R_f C_f$  is connected in parallel to the  
 155 inductor so that the slopes of  $V_{RC}$  are proportional to the induc-  
 156 tor current ramp-up and ramp-down slopes [26]. A small  
 157 resistor ladder is connected between  $V_{RC}$  and ground in order  
 158 to generate a lower voltage signal  $V_{iLsense}$  which falls within  
 159 the input voltage range of the comparator (CMP).  $V_{iLsense}$  is  
 160 fed forward to the corresponding comparators to determine the  
 161 peak-crossing and zero-crossing of the inductor current. Fig. 2  
 162 is a simplified flowchart showing the system-level operation of  
 163 the proposed SIDO buck driver. Suppose identical current flows  
 164 through each of the two LED strings, also referred to as the  
 165 *balanced load* condition, the inductor current  $I_L$  is assigned to  
 166 each string in alternate switching cycles. The working principle  
 167 of the proposed SIDO buck LED driver is represented by the  
 168 timing diagram shown in Fig. 3. During  $D_{1a}T_s$  or  $D_{1b}T_s$ ,  $I_L$   
 169 ramps up with a slope of  $m_1 = (V_g - V_o)/L$  and the inductor  
 170 is charged with a voltage of  $V_L = V_g - V_o$ , where  $V_g$  and  $V_o$   
 171 represent the input voltage and the output voltage, respectively.  
 172 During  $D_{2a}T_s$  or  $D_{2b}T_s$ ,  $I_L$  ramps down with a slope of  $m_2 =$   
 173  $-V_o/L$  and the inductor discharges its current to the correspond-  
 174 ing output capacitor and the LED string until  $I_L$  returns to zero.  
 175 During  $D_{3a}T_s$  or  $D_{3b}T_s$ ,  $I_L$  stays at zero with both  $S_1$  and  $S_2$   
 176 OFF. In the proposed SIDO LED driver, the system clock defines  
 177 the switching frequency. The rising edge of the system clock  
 178 triggers the ON duty cycle ( $D_{1a}T_s, D_{1b}T_s$ ) by charging  
 179 up the inductor during which  $S_1$  is ON and  $S_2$  is OFF. The  
 180



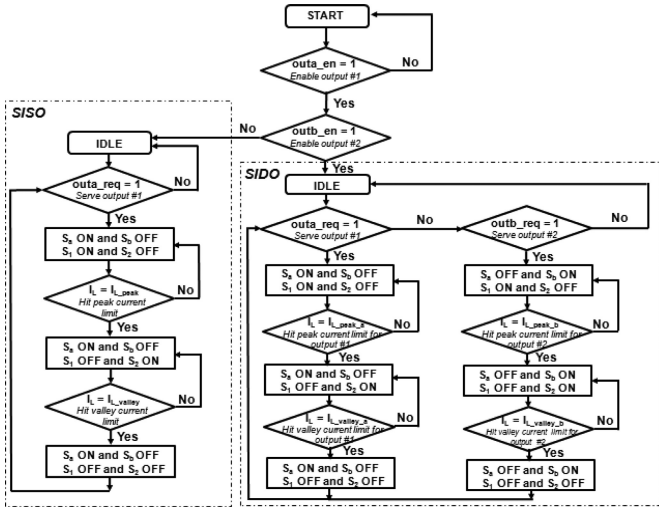


Fig. 2. Simplified flowchart representing the system-level operation of the proposed SIDO buck LED driver.

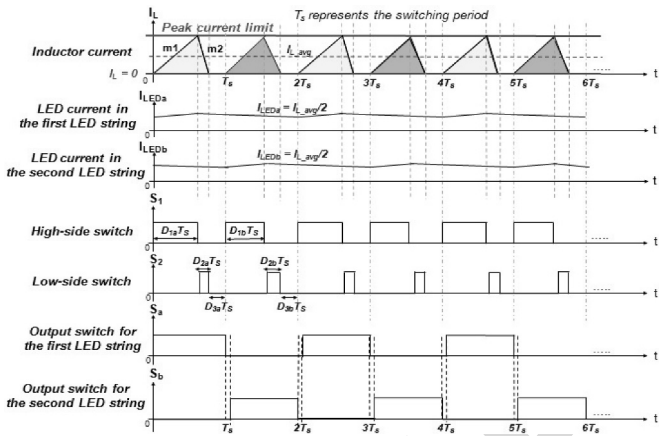


Fig. 3. Timing diagram of the proposed SIDO buck LED driver with balanced load operating in DCM.

181 inductor current continues to increase until it hits the peak  
 182 current limit at which point the buck converter enters  
 183 ( $D_{2a}T_s, D_{2b}T_s$ ) where  $S_1$  is OFF and  $S_2$  is ON. The inductor  
 184 discharges its current to the corresponding output until the  
 185 zero-crossing of the inductor current is detected. The converter  
 186 then enters the idle phase ( $D_{3a}T_s, D_{3b}T_s$ ) during which both  
 187  $S_1$  and  $S_2$  are OFF. The inductor current remains at zero until the  
 188 next rising edge of the system clock arrives and the switching  
 189 sequence repeats itself. The two output switches ( $S_a, S_b$ ) are  
 190 controlled by the FSM as shown in Fig. 4.

191 The state machine is triggered by the rising edge of the system  
 192 clock ( $sysclk$ ) so that the transitions of the output switches  
 193 ( $S_a, S_b$ ) are in sync with the system clock. The input signals  
 194 of the state machine are the output enable signals ( $outa\_en,$   
 195  $outb\_en$ ) and the output request signals ( $outa\_req, outb\_req$ )  
 196 which determine the switching sequence of the two outputs. The  
 197 first LED string is always given a higher priority over the second  
 198 one. For instance, if both strings request service simultaneously,  
 199 i.e.,  $outa\_req = 1$  and  $outb\_req = 1$ ,  $S_a$  is turned ON first and  
 200  $S_b$  remains OFF.  $S_b$  is turned ON only when  $outa\_req = 0$

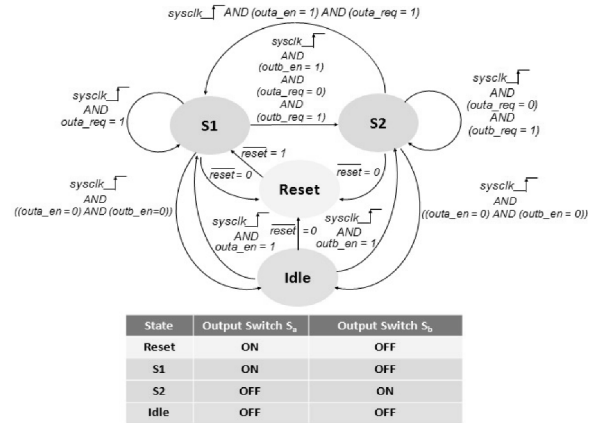


Fig. 4. State diagram of the proposed FSM for controlling the two output switches in SIDO buck LED driver.

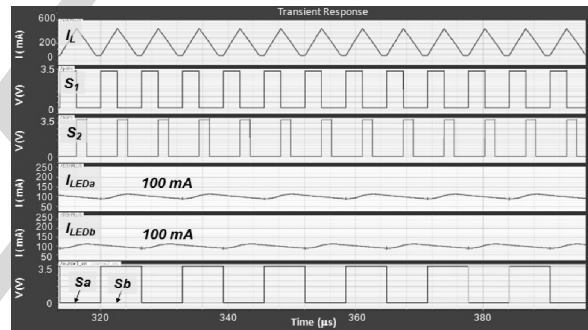


Fig. 5. Simulated steady-state waveforms for the proposed SIDO buck LED driver operating in DCM.

and  $outb\_req = 1$ .  $S_a$  and  $S_b$  must be nonoverlapping to avoid  
 201 undesirable cross conduction between the two LED strings. In  
 202 addition, an enable signal ( $out1en, out2en$ ) is associated with  
 203 either of the two LED strings. It provides the option of shutting  
 204 down any or all of the LED strings, for example, in response to an  
 205 overcurrent fault condition. An overriding signal can also be sent  
 206 from the FSM to the hysteretic controller to disable the high-side  
 207 and low-side power switches accordingly. The FSM-based controller  
 208 can be modified quickly and conveniently to drive multiple LED  
 209 strings in a SIMO configuration by simply adding more states in the  
 210 VHDL or Verilog code. A mixed-signal macromodel of the proposed  
 211 FSM-based digitally controlled SIDO buck switching LED operating  
 212 in DCM is simulated in the time domain using Cadence Spectre [27].  
 213 The FSM is modeled in Verilog RTL and the rest are modeled as  
 214 ideal circuit elements. The simulation model also incorporates  
 215 parasitics such as DCR of the inductor  $L$  and ESR of the output  
 216 capacitors ( $C_{oa}, C_{ob}$ ). For *balanced load* condition, the current  
 217 between the two LED strings is identical and each string consists  
 218 of *two* LEDs connected in series. First, the steady-state  
 219 performance is investigated. Fig. 5 contains the simulated  
 220 steady-state waveforms for the inductor current ( $I_L$ ), the LED  
 221 current ( $I_{LEDa}, I_{LEDb}$ ), and the four switches ( $S_1, S_2, S_a, S_b$ )  
 222 of the proposed SIDO buck LED driver operating in DCM. The  
 223 switching frequency is 156.25 kHz and the input voltage  $V_g$  is  
 224 15 V. The simulation results show that the LED current in either  
 225

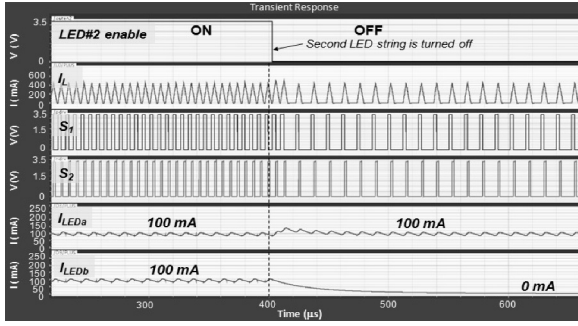


Fig. 6. First LED string remains under regulation without cross regulation when the second LED string is shut down completely.

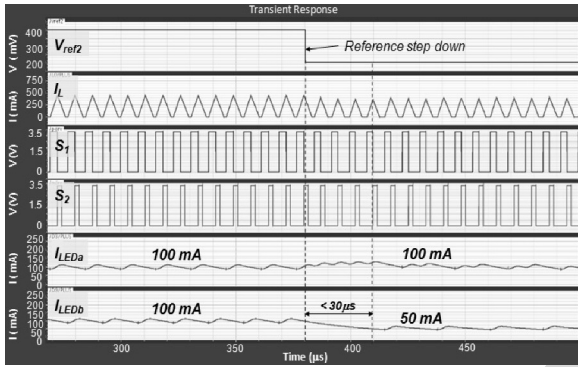


Fig. 7. First LED string remains under regulation without cross regulation despite a reference step in the second LED string from 100 to 50 mA in 20 ns.

227 of the two strings is regulated successfully to the target steady-  
 228 state dc value of 100 mA with a current ripple of 23%<sub>P-P</sub>.  
 229 The steady-state output voltage for the first and second  
 230 LED string is approximately 6.48 V with a voltage ripple of 2.6%<sub>P-P</sub>.  
 231 Second, the stability of the closed-loop system is verified by  
 232 examining its dynamic performance. In the first scenario, the  
 233 second LED string needs to be shut down instantly in response  
 234 to an over-current condition. Fig. 6 shows that despite the im-  
 235 mediate shutdown of the second LED string, the LED current  
 236  $I_{LEDa}$  in the first LED string continues to be regulated suc-  
 237 cessfully at its target nominal value of 100 mA with minimal cross  
 238 regulation. In the second scenario, the second LED string expe-  
 239 riences a reference step of 50 mA, i.e.,  $I_{LEDb}$  transitions from  
 240 100 to 50 mA in 20 ns. Fig. 7 shows that the current in the first  
 241 LED string continues to be regulated at around 100 mA, virtu-  
 242 ally unaffected by the sudden reference step in the other string.  
 243 The second LED string settles to the new nominal current value  
 244 of 50 mA. It demonstrates that the closed-loop system remains  
 245 stable in response to the reference transient in the second string.

246 Unlike conventional backlight LED drivers that use PWM  
 247 dimming transistor connected in series with the LED string [3],  
 248 [8], [28]–[31], the proposed SIDO LED driver takes advantage  
 249 of the existing four switches to perform dimming without re-  
 250 quiring additional switches. When the dimming control signal  
 251 for a particular LED string goes high, certain phases of the in-  
 252 ductor current are skipped so that the average inductor current  
 253 (also the average load current) going into that string is reduced  
 254 accordingly. The digital dimming control signals ( $dim\_ctrl1$ ,

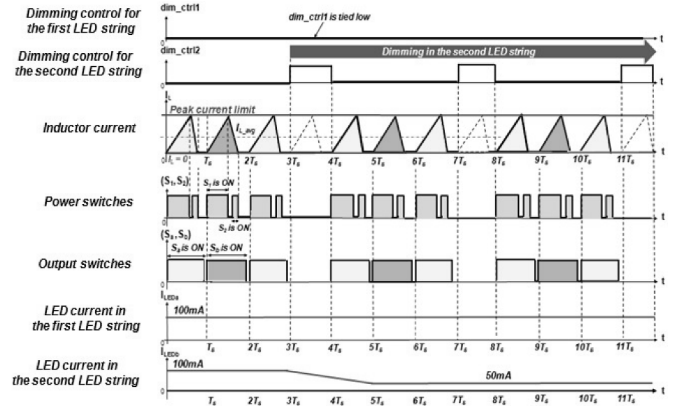


Fig. 8. Proposed digital dimming control in SIDO buck LED driver.

255  $dim\_ctrl2$ ) essentially modulate the dc current level flowing  
 256 through the corresponding LED string. No additional dimming  
 257 transistors in series with the LED string are required, thereby  
 258 leading to a smaller voltage headroom and reduced power loss.  
 259 The only voltage headroom is the voltage across the current-  
 260 sense resistor ( $V_{csa}$ ,  $V_{csb}$ ) which is typically between 0.2 and  
 261 0.4 V. Fig. 8 depicts the timing diagram of the proposed digital  
 262 dimming control scheme. In this particular case, the second LED  
 263 string is dimmed by reducing its current from 100 to 50 mA,  
 264 while the current in the first LED string stays constant at 100 mA.

265 Any combination of LED strings in a SIMO LED driver can  
 266 be dimmed or even shut down momentarily to achieve flexi-  
 267 ble dimming and optimum luminance levels. In addition, it is  
 268 reported in the literature [32]–[34] that a bilevel or  $N$ -level cur-  
 269 rent driving technique for LED dimming improves the luminous  
 270 efficacy of LEDs by introducing a dc offset to the PWM cur-  
 271 rent. The proposed SIDO converter can potentially be used as  
 272 a bilevel LED driver by generating two programmable dc cur-  
 273 rent values for each individual LED string in a time-multiplexed  
 274 fashion. Another major difference between the proposed LED  
 275 driver and the existing ones [3], [8], [28]–[31] is that the former  
 276 provides  $N$  optimized output bus voltage for each individual  
 277 LED string, whereas the latter only uses a common output bus  
 278 shared by all the LED strings. Due to manufacture, process,  
 279 and temperature variations,  $V_F$  in each LED does not match  
 280 perfectly, which means that the voltage drop across each LED  
 281 string differs. Using the proposed SIDO buck LED driver in  
 282 Fig. 1 as an example and assuming the LED current is 100 mA  
 283 in each string, the voltage headroom ( $V_{csa}$ ,  $V_{csb}$ ) is 0.4 V, and  
 284 the voltage drop across each of the two LED strings are  $V_{Fa} =$   
 285 6.0 V and  $V_{Fb} = 7.0$  V, respectively. The output voltages are  
 286  $V_{oa} = 6.4$  V and  $V_{ob} = 7.4$  V. The total power consumption  
 287 of the load  $P_{LOAD}$ , including the LED string and current-sense  
 288 resistor, is  $P_{LOAD} = V_{oa} \times I_{LED} + V_{ob} \times I_{LED} = 1.38$  W. The  
 289 output voltage for each LED string is independently optimized  
 290 based on its corresponding  $V_F$ , resulting in the same voltage  
 291 headroom of 0.4 V for each string. This is different from a con-  
 292 ventional LED driver in which the common output bus voltage  
 293 is usually regulated using the LED string with the maximum  
 294 voltage drop. For the same LED current, the total power con-  
 295 sumption using a conventional LED driver is given by:  $P_{LOAD} =$

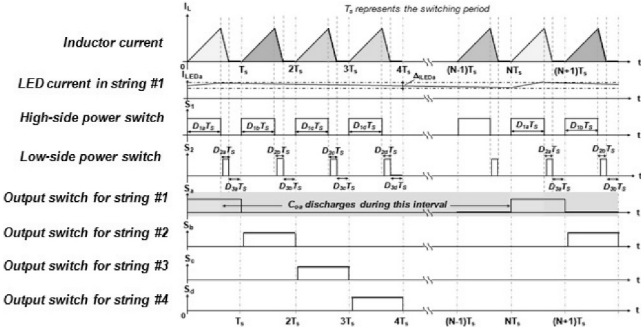


Fig. 9. Timing diagram of the proposed SIMO buck LED driver.

296  $2 \times \max(V_{oa}, V_{ob}) \times I_{LED} = 1.48 \text{ W}$ , which is more than 7%  
 297 higher than that of the proposed driver. The voltage headroom  
 298 for the first LED string increases from 0.4 to 1.4 V, resulting in  
 299 450 mW more power loss or additional 30% efficiency degra-  
 300 dation. Since the output voltage is self-optimized to match the  
 301 total  $V_F$  in each individual LED string in the proposed driver,  
 302 same-colored LEDs from neighboring bins (not only from a  
 303 single bin) with larger  $V_F$  variance can be used which helps  
 304 reduce the LED costs. In the event that a particular application  
 305 demands a total LED current greater than the average inductor  
 306 current, the same time-multiplexing control scheme operating  
 307 in DCM can still be employed either by lowering the switch-  
 308 ing frequency with a higher inductor peak current limit or by  
 309 operating the buck LED driver in pseudocontinuous conduction  
 310 mode (PCCM) [17], [35], [36]. In PCCM, the average inductor  
 311 current is increased by simply adding a nonzero dc offset of  $I_{DC}$   
 312 to that of DCM.

### 313 III. EXTENSION FROM SIDO TO SIMO BUCK LED DRIVER

314 Having demonstrated the feasibility of the proposed SIDO  
 315 buck LED driver, it is natural for us to extend it to SIMO with  
 316  $N$  independently driven LED strings. In particular, the theo-  
 317 retical maximum number of LED strings  $N_{max}$  is determined  
 318 for this SIMO architecture. Fig. 9 shows a timing diagram of  
 319 the inductor current, the two power switches ( $S_1, S_2$ ), and the  
 320 first four output switches ( $S_a, S_b, S_c, S_d$ ) in a SIMO buck LED  
 321 driver. To simplify the analysis, the *balanced load* condition is  
 322 assumed. Based on the time-multiplexing control scheme, en-  
 323 ergy is being transferred from the dc supply to each individual  
 324 output *exactly once* within a total of  $N$  switching phases. For a  
 325 particular output, the corresponding output switch is OFF dur-  
 326 ing  $D_3$ , while the output capacitor discharges to the LED string.  
 327 During the subsequent  $(N - 1) \times T_s$  phases, the output switch  
 328 remains OFF and the output capacitor continues to discharge  
 329 to the corresponding LED string. Hence, the *total* discharging  
 330 time for the output capacitor  $t_{dch}$  can be expressed as

$$t_{dch} = D_3 T_s + (N - 1) T_s = (D_3 + N - 1) T_s. \quad (1)$$

$$\text{For } D_3 = 0, t_{dch} = (N - 1) T_s. \quad (2)$$

331 The proposed SIMO buck LED driver is essentially a  
 332 constant-current regulator which maintains a constant dc cur-  
 333 rent  $I_{LED}$  flowing through the LED string via a closed-loop

current-sense feedback control. For very small variation of for- 334  
 ward voltage around the quiescent point (also known as bias 335  
 point) on the LED's exponential  $I$ - $V$  curve, the dc forward cur- 336  
 rent is assumed to be constant. During  $t_{dch}$  when the output 337  
 switch is OFF, the output capacitor is connected to the LED 338  
 string which acts as a constant-current sink (CCS). Assuming 339  
 ideal capacitor with no ESR (the effect of the ESR will be ex- 340  
 plained later), the voltage across the output capacitor  $v_c(t)$  is the 341  
 same as the output voltage which is expressed as the charge  $q(t)$  342  
 divided by the capacitance value  $C_o$ , i.e., 343

$$v_c(t) = \frac{q(t)}{C_o} = \frac{1}{C_o} \int_0^{t_{dch}} i_c(\tau) d\tau + v_c(0). \quad (3)$$

$$\text{For CCS, } i_c(\tau) = I_{LED}. \quad (4)$$

Combining (3) and (4) and rearranging, we have 344

$$\Delta v_o = \Delta v_c = v_c(t) - v_c(0) = \frac{1}{C_o} (I_{LED} t_{dch}). \quad (5)$$

Hence, the *total* discharging time  $t_{dch}$  can be expressed as 345

$$t_{dch} = \frac{C_o \Delta v_o}{I_{LED}} \quad (6)$$

where  $\Delta v_o$  is the output voltage drop due to the discharging 346  
 of the output capacitor. In general,  $\Delta v_o$  is assumed to be 347  
 reasonably small relative to the output voltage. The LED ripple 348  
 current  $\Delta i_{LED}$  usually ranges from 10%<sub>P-P</sub> to 40%<sub>P-P</sub> of the 349  
 dc forward current as recommended by the LED manufactur- 350  
 ers [37], [38]. For a particular  $\Delta i_{LED}$ , the corresponding voltage 351  
 ripple  $\Delta v_{LED}$  at the chosen bias point can be readily obtained 352  
 from the exponential  $I$ - $V$  curve. Suppose each LED string con- 353  
 tains a total of  $n$  LEDs connected in series. The output voltage 354  
 ripple  $\Delta v_o$  is, therefore, the sum of the voltage ripple across 355  
 the LED string and the voltage ripple across the current-sense 356  
 resistor, i.e.,  $\Delta v_o = n \times \Delta v_{LED} + \Delta v_{cs}$ . Suppose  $\Delta v_{o,max}$  rep- 357  
 represents the *maximum* output voltage ripple allowed. Equation (6) 358  
 can, therefore, be rewritten as 359

$$t_{dch} \leq \frac{C_o \Delta v_{o,max}}{I_{LED}}. \quad (7)$$

Substituting (1) into (7), we have 360

$$\begin{aligned} (D_3 + N - 1) T_s &\leq \frac{C_o \Delta v_{o,max}}{I_{LED}} \Rightarrow N \\ &\leq \frac{C_o \Delta v_{o,max}}{I_{LED} T_s} + 1 - D_3. \end{aligned} \quad (8)$$

Hence, the theoretical maximum possible number of LED 361  
 strings in SIMO,  $N_{max}$ , is given by 362

$$N_{max} = \frac{C_o \Delta v_{o,max}}{I_{LED} T_s} + 1 - D_3 = \frac{C_o \Delta v_{o,max}}{I_{LED} T_s} + D_1 + D_2. \quad (9a)$$

Since  $N_{max}$  is an integer value, the *floor*( $\cdot$ ) function is used to 363  
 round the result down to the closest integer. Hence, (9a) becomes 364

$$N_{max} = \text{floor} \left( \frac{C_o \Delta v_{o,max} + I_{LED} T_s (1 - D_3)}{I_{LED} T_s} \right). \quad (9b)$$

Equation (9b) represents a general formula for determining the 365  
 scalability limit of a SIMO buck LED driver operating in DCM 366

and is referred to as a *scalable DCM-based SIMO scheme* for the sake of our ensuing discussion. In particular, when  $D_3 = 0$ , the SIMO buck LED driver operates in boundary conduction mode (BCM). Hence, (9a) and (9b) become (10a) and (10b), respectively. Also,  $N_{\max}$  in BCM is greater than or equal to that in DCM for the same set of design parameter values

$$N_{\max} = \frac{C_o \Delta v_{o \max}}{I_{\text{LED}} T_s} + 1 \quad (10a)$$

$$N_{\max} = \text{floor} \left( \frac{C_o \Delta v_{o \max}}{I_{\text{LED}} T_s} + 1 \right). \quad (10b)$$

For a single-output buck converter, the average inductor current is identical to the load current. Due to the nature of the time-multiplexing control scheme in the proposed SIMO converter, the average inductor current  $I_{L_{\text{avg}}}$  is the *sum* of the individual load current  $I_{\text{LED}}$  in each LED string. Assuming balanced load condition,  $I_{L_{\text{avg}}} = N \times I_{\text{LED}}$ , where  $N$  is the total number of LED strings. The average inductor current reaches its maximum value in BCM, resulting in a maximum transfer of power [16]. Since the current in each LED string remains the same, a theoretical upper bound of the total achievable number of LED strings in SIMO can be expressed as

$$N_{\max} = \frac{I_{L_{\text{avg-max}}}}{I_{\text{LED}}}. \quad (11)$$

By simple geometry,  $I_{L_{\text{avg-max}}}$  is given by the following equation [39]:

$$I_{L_{\text{avg-max}}} = \frac{m_1 D_1 T_s}{2} = \frac{(V_g - V_o) D_1 T_s}{2L}. \quad (12)$$

By substituting (12) into (11) and rearranging,  $T_s$  can be expressed as

$$T_s = \frac{2LN_{\max}I_{\text{LED}}}{D_1(V_g - V_o)}. \quad (13)$$

Now, by substituting (13) into (10a) and rearranging, we have

$$2LI_{\text{LED}}^2 N_{\max}^2 - 2LI_{\text{LED}}^2 N_{\max} - C_o \Delta v_{o \max} (V_g - V_o) D_1 = 0. \quad (14)$$

Equation (14) is a quadratic equation in  $N_{\max}$ . The discriminant  $\Delta$  of (14) can be expressed as

$$\Delta = 4L^2 I_{\text{LED}}^4 + 8LI_{\text{LED}}^2 C_o \Delta v_{o \max} (V_g - V_o) D_1 > 0. \quad (15)$$

Since  $(V_g - V_o) > 0$  for a buck switcher, the discriminant in (15) is always a positive number which implies that (14) has two real roots as given by

$$r_1, r_2 = \frac{2LI_{\text{LED}}^2 \pm \sqrt{\Delta}}{4LI_{\text{LED}}^2}. \quad (16)$$

Since  $N_{\max}$  must be a *positive integer*, the negative root is eliminated, leaving only the positive root, i.e.,

$$N_{\max\_BCM} = \text{floor} \left( \frac{1}{2} \times \left[ 1 + \sqrt{1 + \frac{2C_o \Delta v_{o \max} V_o (V_g - V_o)}{LI_{\text{LED}}^2 V_g}} \right] \right) \quad (17)$$

Equation (17) defines the theoretical maximum total number of outputs in SIMO operating in BCM. It is referred to as a

*scalable BCM-based SIMO scheme* which is a special case of *scalable DCM-based SIMO scheme*. In fact, it is observed that (11) is also valid for the case of DCM. By simple geometry, the switching period  $T_s$  in DCM can be expressed as

$$T_s = \frac{2LN_{\max}I_{\text{LED}}}{D_1(D_1 + D_2)(V_g - V_o)}. \quad (18)$$

Realizing that the same calculations that lead to (17) for the case of BCM can also be performed in DCM, the theoretical maximum total number of LED strings in a SIMO converter operating in DCM can, therefore, be written as<sup>1</sup>

$$N_{\max\_DCM} = \text{floor} \left( \frac{1}{2} \times (1 - D_3) \times \left[ 1 + \sqrt{1 + \frac{2C_o \Delta v_{o \max} (V_g - V_o) D_1}{LI_{\text{LED}}^2 (1 - D_3)}} \right] \right). \quad (19)$$

Notice that for the case of BCM,  $D_3 = 0$  and  $D_1 = V_o / V_g$ , (19) reduces to (17). Hence, (19) represents the generalized formula for the theoretical maximum total number of outputs in SIMO which is applicable to either BCM or DCM. It is also interesting to note that the average inductor current in DCM is smaller than (or equal to) that in BCM. As a result, for the same LED current, the theoretical maximum achievable number of outputs in SIMO operating in DCM is no greater than that in BCM, i.e.,  $N_{\max\_DCM} \leq N_{\max\_BCM}$ . In reality, the ESR of the output capacitor needs to be taken into consideration. Any current flowing through the output capacitor  $C_o$  must also flow through the  $R_{\text{ESR}}$ , resulting in an additional voltage drop of  $\Delta V_{\text{ESR}} = I_{\text{LED}} \times R_{\text{ESR}}$ . Hence,  $\Delta v_o$  can be expressed as

$$\Delta v_o = \Delta v_c + \Delta v_{\text{ESR}} = \Delta v_c + I_{\text{LED}} \times R_{\text{ESR}}. \quad (20)$$

Rearranging the terms in (20), we have

$$\Delta v_c = \Delta v_o - I_{\text{LED}} \times R_{\text{ESR}}. \quad (21)$$

Hence, (17) and (19) are modified slightly to become (22) and (23), respectively: BCM:

$$N_{\max\_BCM} = \text{floor} \left( \frac{1}{2} \times \left[ 1 + \sqrt{1 + \frac{2C_o V_o (\Delta v_{o \max} - I_{\text{LED}} R_{\text{ESR}}) (V_g - V_o)}{LI_{\text{LED}}^2 V_g}} \right] \right) \quad (22)$$

DCM:

$$N_{\max\_DCM} = \text{floor} \left( \frac{1}{2} \times (1 - D_3) \times \left[ 1 + \sqrt{1 + \frac{2C_o (\Delta v_{o \max} - I_{\text{LED}} R_{\text{ESR}}) (V_g - V_o) D_1}{LI_{\text{LED}}^2 (1 - D_3)}} \right] \right). \quad (23)$$

The presence of  $R_{\text{ESR}}$  in (22) and (23) reduces the theoretical maximum achievable number of outputs in SIMO. Therefore,

<sup>1</sup>In DCM,  $D_1$  can be expressed as:  $D_1 = M \sqrt{\frac{K}{1-M}}$ , where  $M = \frac{V_o}{V_g}$  and  $K = \frac{2L}{R_L T_s} = \frac{2LI_{\text{LED}}}{V_o T_s}$  [39].

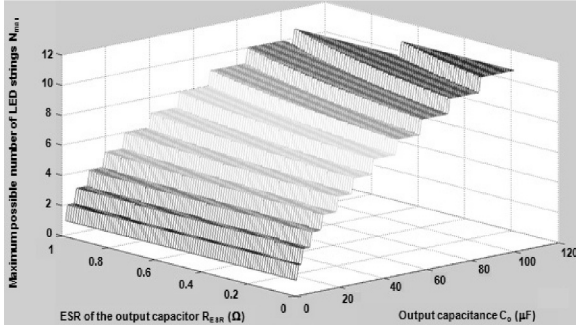


Fig. 10. Theoretical maximum achievable number of LED strings ( $N_{max}$ ) versus the output capacitance ( $C_o$ ) and the capacitor ESR ( $R_{ESR}$ ) for the scalable BCM-based SIMO scheme.

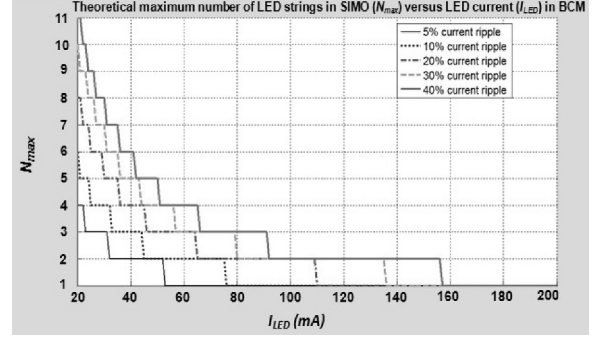


Fig. 11. Plot of theoretical maximum number of LED strings in SIMO ( $N_{max}$ ) versus the LED current ( $I_{LED}$ ) in the scalable BCM-based SIMO scheme.

425 it is always recommended to choose an output capacitor with a  
426 smaller ESR, whenever possible. Fig. 10 shows the theoretical  
427 maximum total number of LED strings versus the output cap-  
428 acitance and capacitor ESR for the scalable BCM-based SIMO  
429 scheme, given a LED current of 80 mA and a maximum ripple  
430 current requirement of 40%<sub>P-P</sub>.

431 Intuitively, for a particular LED current, an increasing number  
432 of outputs can be achieved by using a larger output capacitor  
433 with the same ESR value. For instance, if the output capacitance  
434 is increased from 4.7 to 22 μF (the ESR remains at 100 mΩ),  
435 the theoretical model based on (22) suggests that the maximum  
436 total number of LED strings can be increased from three to six.  
437 It is also interesting to note that the maximum number of outputs  
438 in SIMO has a stronger dependence on the output capacitance  
439 than the capacitor ESR, as shown in Fig. 10.

440 On the other hand, it is useful to study how the LED current  
441 affects the maximum achievable number of outputs in SIMO.  
442 As an example, assuming balanced load and two LEDs con-  
443 nected in series per string, a scalable BCM-based SIMO scheme  
444 is investigated with these parameter values:  $L = 47 \mu\text{H}$ ,  $C_o =$   
445  $4.7 \mu\text{F}$ ,  $R_{ESR} = 100 \text{ m}\Omega$ ,  $V_g = 15 \text{ V}$ , and  $V_o = 6.4 \text{ V}$ . The  
446 relationship between  $N_{max}$  and  $I_{LED}$  can be obtained by using  
447 (22) for different values of output voltage ripple  $\Delta v_{o\_max}$ .  
448 Based upon the  $I$ - $V$  curve and/or SPICE model of the particular  
449 LED used, the corresponding output voltage ripple  $\Delta v_{o\_max}$  can  
450 be determined from the LED current ripple requirement  $\Delta i_{LED}$ .  
451 The proposed design uses white LED [40] which is the target for  
452 LCD backlighting applications. For instance, a 20%<sub>P-P</sub> current  
453 ripple corresponds to around 2%<sub>P-P</sub> voltage ripple and a 40%<sub>P-P</sub>  
454 current ripple corresponds to around 4%<sub>P-P</sub> voltage ripple.  
455 Fig. 11 shows a plot of  $N_{max}$  versus  $I_{LED}$  for  $\Delta i_{LED}$  rang-  
456 ing from 5%<sub>P-P</sub> to 40%<sub>P-P</sub>. This plot is beneficial to a practical  
457 SIMO design in two ways. First, for a given LED current and  
458 current ripple requirement, the theoretical maximum number  
459 of LED strings viable under the scalable BCM-based SIMO  
460 scheme can be extracted directly from the plot. Second, the

461 maximum LED current allowed in order for a SIMO to remain  
462 at the same scaling level can also be obtained from the plot. For  
463 instance, given a 20% current ripple requirement (i.e.,  $\Delta i_{LED} =$   
464  $20\%_{P-P}$ ), a SIMO (dual-string) configuration is possible as long  
465 as the LED current in each string is no more than 110 mA. In  
466 the event that an application demands an LED current greater  
467 than 110 mA, two options can be considered: 1) Relax the cur-  
468 rent ripple requirement whenever possible. A wider tolerance  
469 in  $\Delta i_{LED}$  is generally acceptable since the ripple frequency is  
470 too high for the human eye to detect. 2) Operate the SIMO buck  
471 LED driver in PCCM [17], [35], [36]. In PCCM, the floor of  
472 the inductor current is raised by a nonzero dc offset  $I_{DC}$  which  
473 distinguishes it from DCM. The proposed theoretical model can  
474 be extended to PCCM by adding a dc component to the aver-  
475 age inductor current. By going through similar calculations as  
476 in DCM, the theoretical maximum number of outputs in SIMO  
477 operating in PCCM is given by (24), as shown at the bottom of  
478 the page. It is interesting to note that (24) continues to apply to  
479 the cases of DCM and BCM. For instance, in DCM,  $I_{DC} = 0$   
480 and (24), therefore, reduces to (23).

481 In the event of unbalanced load with unequal current among  
482 the LED strings, the scalable DCM- or BCM-based SIMO  
483 scheme continues to hold. The only change is to replace  $I_{LED}$   
484 in (22) and (23) by  $\max(I_{LED})$ , where  $\max(I_{LED})$  denotes the  
485 largest LED current among all the LED strings. In other words,  
486 the maximum number of LED strings that can be realized in  
487 a SIMO buck LED driver is constrained by the largest LED  
488 current. Generally speaking, the input voltage  $V_g$ , output volt-  
489 age  $V_o$ , and the current ripple requirement are typically fixed  
490 parameters defined in the design specification. Without making  
491 any hardware changes (i.e.,  $L$  and  $C_o$  values are fixed), the pri-  
492 mary design variable in (22) and (23) is the LED current  $I_{LED}$ .  
493 In fact, the LED current is the dominant factor for determining  
494 the maximum possible number of outputs under the scalable  
495 DCM-/BCM-based SIMO scheme. By knowing the maximum  
496 LED current required for a particular application, the theoretical

$$N_{max\_PCCM} = \text{floor} \left( \frac{1}{2I_{LED}} \times [(I_{DC} + (1 - D_3) I_{LED}) \times \left[ 1 + \sqrt{1 + \frac{2C_o(\Delta v_{o\_max} - I_{LED} R_{ESR})(V_g - V_o) D_1(1 - D_3)}{L [I_{DC} - (1 - D_3) I_{LED}]^2}} \right] \right) \right). \quad (24)$$

TABLE I  
DESIGN SPECIFICATION OF A SISO BUCK LED DRIVER IN DCM

Design Parameter	Value	Unit
Input Voltage ( $V_g$ )	15	V
Output Voltage ( $V_o$ )	6.32	V
LED Forward Current ( $I_{LED}$ )	80	mA
Switching Frequency ( $f_s$ )	100	kHz
Inductor ( $L$ )	47	$\mu$ H
Output Capacitor ( $C_o$ )	4.7	$\mu$ F
ESR of Output Capacitor ( $R_{ESR}$ )	100	m $\Omega$
Maximum LED Current Ripple ( $\Delta i_{LED}$ )	40	% <sub>P-P</sub>
Maximum Output Voltage Ripple ( $\Delta v_o$ )	4	% <sub>P-P</sub>
Duty Ratio of Idle Phase ( $D_3$ )	$\geq 10$	%

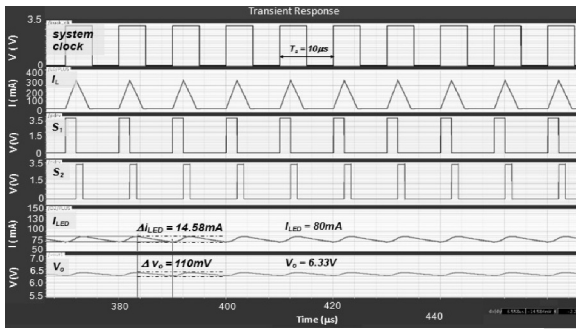


Fig. 12. Simulated steady-state waveforms for the SISO buck LED driver based on the design specification in Table I.

497 maximum achievable number of independently driven LED  
498 strings can be estimated in advance.

#### IV. SIMULATION RESULTS

500 Ideal macromodels based on the *scalable DCM-based SIMO*  
501 *scheme* were constructed and simulated in Cadence Spectre [27]  
502 in order to compare with the theoretical results in Section III. The  
503 design specification of a single-inductor single-output (SISO)  
504 buck converter is shown in Table I. The theoretical model based  
505 on (23) suggests that  $N_{max\_DCM} = 1$ , meaning only one LED  
506 string is viable. Fig. 12 shows the simulated steady-state wave-  
507 forms of the inductor current  $I_L$ , the LED currents  $I_{LED}$ , and  
508 the output voltages  $V_o$  of a SISO buck LED driver. The simu-  
509 lated steady-state LED current  $I_{LED}$  is approximately 80 mA  
510 which meets the design target. The simulated LED current ripple  
511  $\Delta i_{LED}$  is 18%<sub>P-P</sub> (also, the output voltage ripple  $\Delta v_o$  is  
512 1.7%<sub>P-P</sub>), which satisfies the maximum ripple requirement.  
513 Now, the SISO buck LED driver is transformed into SIDO  
514 by adding a second LED string. Fig. 13 shows the simulated  
515 steady-state waveforms from the resulting SIDO LED driver.

516 Despite the fact that the steady-state LED current in either  
517 string remains at 80 mA, the LED current ripple is more than  
518 40%<sub>P-P</sub> which violates the maximum ripple current require-  
519 ment. Hence, the simulation results show that SIDO is not viable  
520 based on the design requirement which is consistent with the  
521 theoretical result. By increasing the switching frequency from

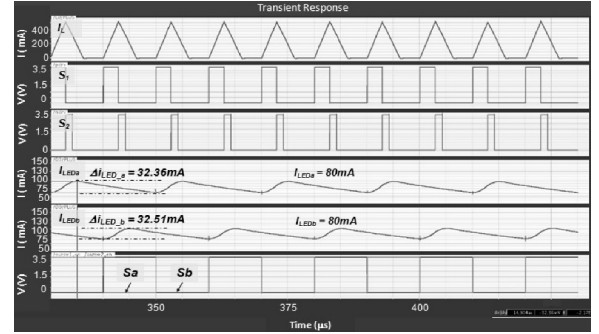


Fig. 13. Simulated steady-state waveforms showing SIDO is not viable since the 30%<sub>P-P</sub> maximum current ripple requirement is violated.

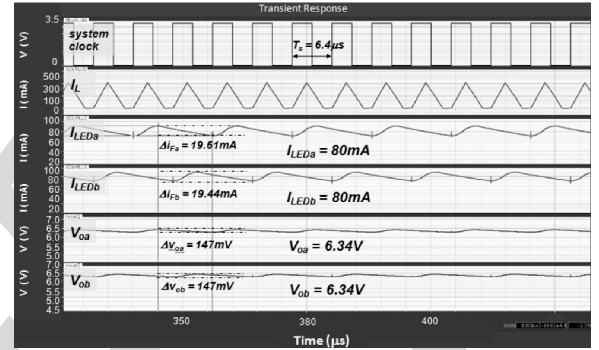


Fig. 14. Simulated steady-state waveforms showing SIDO is possible by increasing the switching frequency from 100 to 156.25 kHz.

100 to 156.25 kHz and keeping other parameters unchanged, 522  
 $N_{max\_DCM} = 2$  from (23). Fig. 14 shows the simulated wave- 523  
forms for the corresponding signals in a SIDO buck LED driver. 524  
The simulated LED current ripple  $\Delta i_{LED}$  is 24%<sub>P-P</sub> and the 525  
corresponding output voltage ripple  $\Delta v_o$  is 2.3%<sub>P-P</sub>, both of which 526  
satisfy their corresponding maximum ripple requirement. Con- 527  
sequently, both the theoretical and simulation results show that 528  
by increasing the switching frequency, a SIDO buck LED driver 529  
in DCM is feasible. 530

531 A third LED string is added to the SIDO buck LED driver to  
532 transform it into SIMO consisting of three independently driven  
533 LED strings. The LED current in each string remains unchanged  
534 at 80 mA as in the SISO or SIDO case. According to Fig. 11,  
535 the theoretical model suggests that for  $I_{LED} = 80$  mA, a *scal-*  
536 *able BCM-based SIMO* scheme with a maximum of *three* LED  
537 strings is feasible under the 40%<sub>P-P</sub> current ripple constraint.  
538 The switching period  $T_s$  is chosen to be 6  $\mu$ s using (13) which  
539 corresponds to a switching frequency of 166.67 kHz. Fig. 15  
540 shows the simulated waveforms from the resulting SIMO buck  
541 LED driver. The simulated LED current ripple  $\Delta i_{LED}$  is around  
542 35%<sub>P-P</sub> and the output voltage ripple  $\Delta v_o$  is 3.5%<sub>P-P</sub>, both of  
543 which satisfy their respective maximum ripple constraint. As a  
544 sanity check, the theoretical model based on (22) indeed sug-  
545 gests that a maximum possible number of *three* independently  
546 driven LED strings can be achieved in the *scalable BCM-based*  
547 *SIMO* scheme. Hence, it is shown that the simulation result  
548 agrees with the corresponding theoretical result. On the other  
549 hand, it is important to examine the transient performance of the

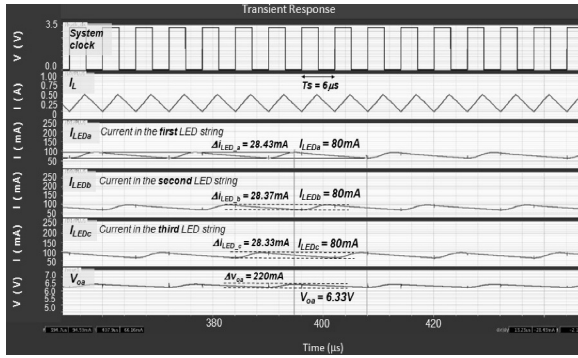


Fig. 15. Simulated steady-state waveforms of a three-string SIMO buck LED driver operating in BCM.

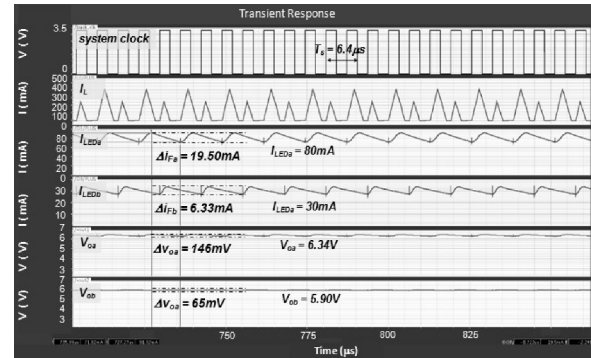


Fig. 17. Simulated steady-state waveforms of a SIDO buck LED driver with unbalanced load.

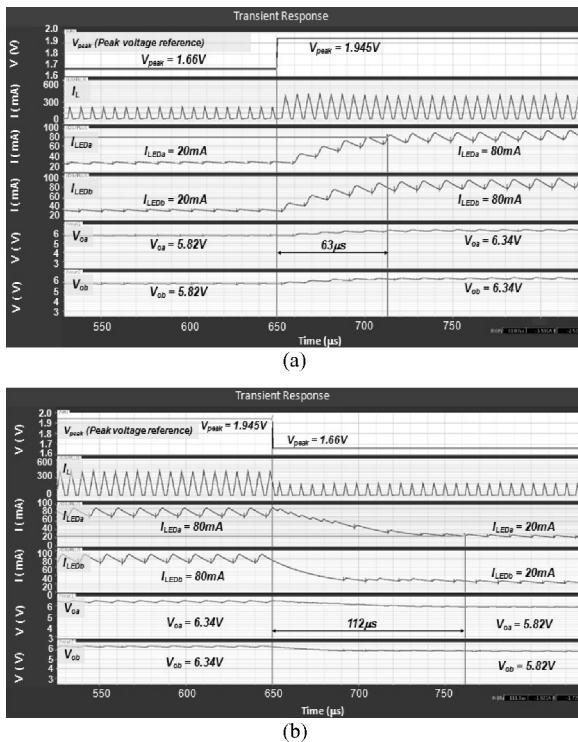


Fig. 16. Simulated transient waveforms for (a) peak reference step-up and (b) peak reference step-down response.

550 proposed SIDO buck LED driver. The LED current is changed  
 551 by adjusting the peak limit of the inductor current. By stepping  
 552 up the peak voltage reference ( $V_{peak}$  in Fig. 1) from 1.660 to  
 553 1.945 V in 400 ns, the peak inductor current limit is increased  
 554 by approximately 200 mA, leading to an increase in the nominal  
 555 LED current from 20 to 80 mA. The reference voltages  
 556 ( $V_{refa}$ ,  $V_{refb}$ ) are also stepped up from 100 to 340 mV in order  
 557 to maintain the same load current between the two LED strings.  
 558 Conversely, by stepping down  $V_{peak}$  from 1.945 to 1.660 V,  
 559 the LED current is reduced from 80 to 20 mA. Fig. 16 shows  
 560 the simulated transient behavior for the peak voltage reference  
 561 step-up and step-down response.

562 In the case of step-up reference response, the LED current in  
 563 either string settles to the steady-state nominal value of 80 mA  
 564 within 63  $\mu$ s. The output voltage reaches its target steady-state

value of 6.34 V. In the case of step-down reference response, 565  
 the LED current in either string settles to the steady-state nominal 566  
 value of 20 mA in less than 112  $\mu$ s. The output voltage 567  
 settles to its new steady-state value of 5.82 V without oscillations. 568  
 Hence, the simulation results show that the closed-loop 569  
 system remains in stable condition in response to a peak voltage 570  
 reference transient. 571

572 The effectiveness of the proposed SIDO converter to drive  
 573 unbalanced load is also investigated. As an example, the first  
 574 and second LED strings require an average current value of 80  
 575 and 30 mA, respectively. Unlike the balanced load case with  
 576 a constant peak inductor current limit, two distinct peak current  
 577 limits are employed for unbalanced load such that two  
 578 different average inductor (or load) current values can be gener-  
 579 ated in alternate clock cycles. Fig. 17 depicts the simulated  
 580 steady-state waveforms from the SIDO buck LED driver with  
 581 unbalanced load. The simulation results show that the first and  
 582 second LED strings are regulated with an average current value  
 583 of 80 and 30 mA, respectively. For the first string, the simu-  
 584 lated current ripple is 24.38%<sub>P-P</sub> and the output voltage ripple  
 585 is 2.3%<sub>P-P</sub>. Also, for the second string, the simulated current  
 586 ripple is 21.1%<sub>P-P</sub> and the output voltage ripple is 1.1%<sub>P-P</sub>.  
 587 Either string meets the maximum ripple requirements. The simu-  
 588 lation results demonstrate that the proposed SIDO converter is  
 589 capable of delivering unequal currents to the two LED strings  
 590 simultaneously. 591

## V. EXPERIMENTAL RESULTS

592 The proposed SIDO buck LED driver was implemented on  
 593 a field-programmable gate array (FPGA)-based hardware proto-  
 594 type in accordance with the design specification provided in  
 595 Table I. The switching frequency is increased to 156.25 kHz in  
 596 order to satisfy the LED current ripple requirement. A photo of  
 597 the experimental setup is shown in Fig. 18. The power stage of  
 598 the buck converter consists of discrete ICs from International  
 599 Rectifier such as power MOSFETs (IRF7828), dual-channel  
 600 gate driver (IR2110), and output switches (IRF9388), as well as  
 601 surface-mount inductor and low-ESR capacitors. In actual im-  
 602 plementation, the top level of the proposed digital controller is  
 603 partitioned into two major functional blocks. The functionality  
 604 of the first block is to control the switching action of the power

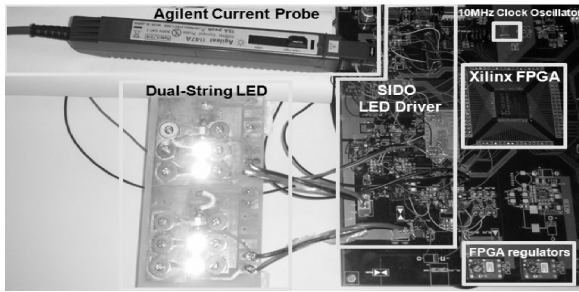


Fig. 18. Experimental setup for the proposed SIDO buck LED driver.

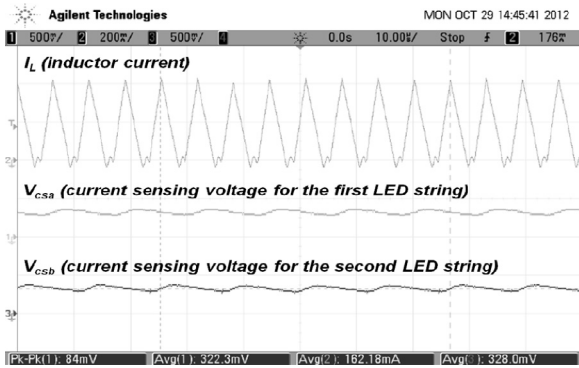


Fig. 19. Measured waveforms for inductor current and current sense feedback voltage.

605 stage by detecting the peak-crossing and zero-crossing events of the inductor current. It was implemented in hierarchical gate-level schematics using primitives and macros available from the Xilinx Spartan-3 Generation library. Dead-time logic is included to prevent shoot-through current of the power switches. The second logical block is used to control the switching sequence of the two output switches by continuously monitoring the current-sense feedback signals. It was modeled as an FSM in Verilog RTL. Only one of the two output switches can be ON and the other must be OFF per switching cycle. Dead-time logic is also added to prevent cross conduction between outputs. The two logical blocks are synchronized by the system clock to ensure that the high-side power switch and the output switches are triggered from the same clock edge. The entire digital controller was implemented with Xilinx Spartan-3E (XC3S250E) FPGA. The quasi-hysteretic control logic was realized using 4-ns fast comparators (AD8611 from Analog Devices) and semicustom synchronous logic.

623 Using a current sensing resistor of  $4\ \Omega$  and reference voltage of 320 mV, the target current in each of the two LED strings is 80 mA. Fig. 19 shows the current sensing feedback voltage ( $V_{CSA}$ ,  $V_{CSB}$ ) from which the corresponding average load current can be obtained, i.e.,  $I_{LED} = V_{CS}/R_{CS}$ . The average inductor current is measured to be 162 mA, which is the sum of the load currents in both LED strings. The average current values in the first and second LED string are measured to be around 80.6 and 82 mA, respectively. The measured LED current ripple  $\Delta I_{LED}$  in either string is around 26%<sub>P-P</sub>, which is reasonably close to the simulated current ripple of 24%<sub>P-P</sub>. In addition, the nominal output voltages in the first and second string are

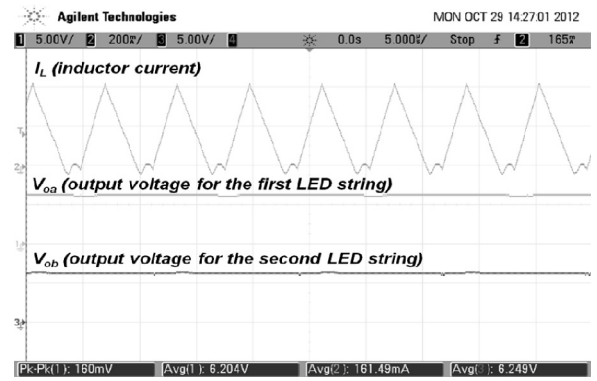


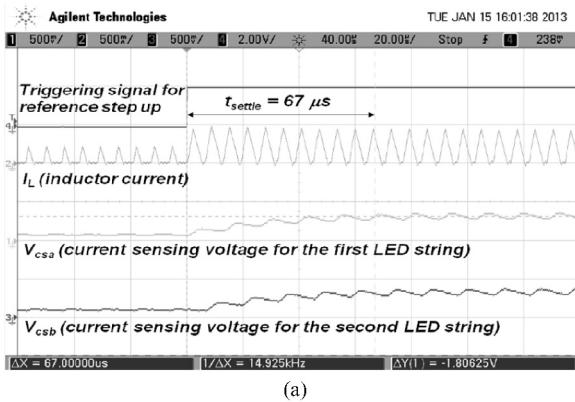
Fig. 20. Measured waveforms for inductor current and output voltage in either LED string.

635 measured to be 6.204 and 6.249 V, respectively, as shown in 636  
 637 Fig. 20. Under this balanced load condition, the measured current and voltage values are in close agreement between the two LED strings. The output voltage ripple is also measured to be around 2.57%<sub>P-P</sub>, compared to 2.3%<sub>P-P</sub> from simulation. Therefore, the experimental results are shown to be consistent with the corresponding simulation ones. On the other hand, the measured power conversion efficiency of the proposed SIDO converter is 80% which is comparable to conventional driving topologies [41]. The efficiency can be further increased by employing a current-sensing resistor with a smaller value.

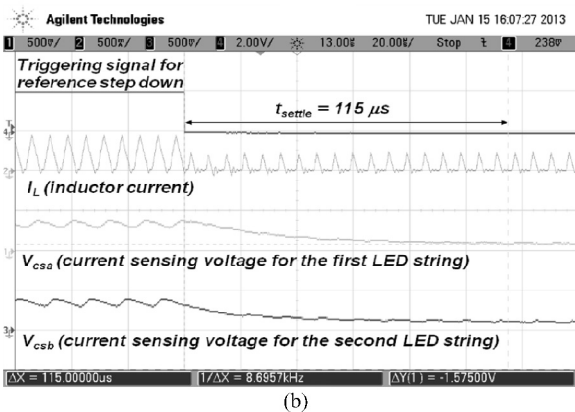
642 The transient response of the proposed SIDO buck LED driver is verified experimentally by measuring its peak voltage reference step response. An 8-bit digital-to-analog converter (AD558 from Analog Devices) is used to enable programming of the peak voltage reference  $V_{PEAK}$  and the current-sense voltage references ( $V_{REFA}$ ,  $V_{REFB}$ ) by the Xilinx FPGA. The measured waveforms of the inductor current and the voltage at the current sensing nodes in response to a peak voltage reference step are shown in Fig. 21. The settling time of the transient response is also measured and compared with the simulated settling time. For the step-up response, it is observed that the current-sensing voltage  $V_{CSA}$  in the first LED string steps up from 81.8 to 325.4 mV, which corresponds to an increase in the average load current from 20.5 to 81.3 mA. Similarly, the current-sensing voltage  $V_{CSB}$  in the second LED string steps up from 94.1 to 327.6 mV, which corresponds to an increase in the average load current from 23.5 to 81.9 mA. The settling time for the step-up response is measured to be 67  $\mu$ s, compared to 63  $\mu$ s from simulation. The measured results for the step-down response are the reverse of those from the step-up response. The only difference is that it takes longer for the step-down transient to settle. The settling time for the step-down response is measured to be 115  $\mu$ s, compared to 112  $\mu$ s from simulation. The measured settling times are shown to be very close to the simulated ones. The experimental results confirm that the system remains in stable condition when it is perturbed by the peak voltage reference transient.

673 The unbalanced load scenario in the proposed SIDO buck LED driver is also verified experimentally. The measured average load current values in the first and second LED string are 674 675





(a)



(b)

Fig. 21. Measured transient waveforms in response to (a) peak reference step-up and (b) peak reference step-down.

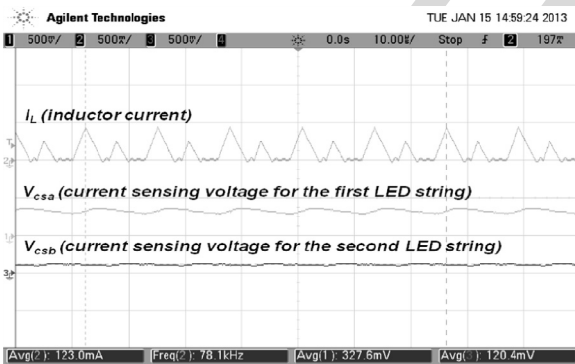


Fig. 22. Measured waveforms for inductor current and current sense voltages.

676 around 81.9 and 30.1 mA, respectively. Fig. 22 shows the measured  
 677 waveforms for the inductor current and the current-sensing  
 678 voltage per string. The inductor current waveform indicates that  
 679 the proposed driver operates in DCM with *two* distinct peak  
 680 current limits. Fig. 23 shows the measured inductor current and  
 681 the output voltage in either string. The measured output voltage  
 682 values in the first and second LED string are 6.22 and 5.70 V,  
 683 respectively. The experimental results demonstrate that the proposed  
 684 driver is capable of driving two independent LED strings  
 685 concurrently with different load current.

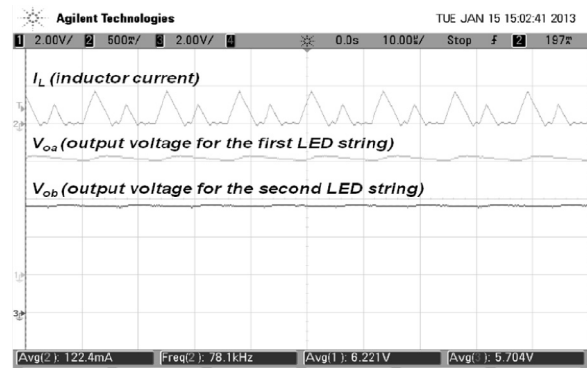


Fig. 23. Measured waveforms for inductor current and output voltages.

## VI. CONCLUSION

The proposed SIDO buck LED driver was implemented in  
 FPGA-based hardware. The experimental results correlate well  
 with simulation ones. The scalability of the proposed SIDO buck  
 LED driver to SIMO is closely examined. A general formula  
 for determining the theoretical maximum achievable number of  
 LED strings in SIMO is derived. The simulation results were  
 shown to be consistent with those obtained from the theoretical  
 model for the same design parameter values. The quasi-hysteretic  
 digital control scheme does not require loop compensation which  
 simplifies the control loop design and reduces component count.  
 In addition, the proposed SIMO architecture offers the advantage  
 of driving a larger number of parallel LED strings without being  
 limited by the maximum current rating of the LED. It also enables  
 dimming for the LED strings without additional dimming transistors.  
 Local bus voltage and current optimization in each individual LED  
 string compensates for the variability of the LED's forward voltage,  
 which reduces power loss and enables mixing of white LEDs from  
 different bins to lower LED costs.

## REFERENCES

- [1] C.-Y. Hsieh, C.-Y. Yang, and K.-H. Chen, "A charge-recycling buck-store and boost-restore (BSBR) technique with dual outputs for RGB LED backlight and flashlight module," *IEEE Trans. Power Electron.*, vol. 24, no. 8, pp. 1914–1925, Aug. 2009.
- [2] S.-Y. Lee, J.-W. Kwon, H.-S. Kim, M.-S. Choi, and K.-S. Byun, "New design and application of high efficiency LED driving system for RGB-LED backlight in LCD display," in *Proc. 37th IEEE Power Electron. Spec. Conf.*, 2006, pp. 1–5.
- [3] H.-J. Chiu, Y.-K. Lo, J.-T. Chen, S.-J. Cheng, C.-Y. Lin, and S.-C. Mou, "A high-efficiency dimmable led driver for low-power lighting applications," *IEEE Trans. Ind. Electron.*, vol. 57, no. 2, pp. 735–743, Feb. 2010.
- [4] C.-H. Liu, C.-Y. Hsieh, Y.-C. Hsieh, T.-J. Tai, and K.-H. Chen, "SAR-Controlled adaptive off-time technique without sensing resistor for achieving high efficiency and accuracy led lighting system," *IEEE Trans. Circuits Syst. I, Reg. Papers*, vol. 57, no. 6, pp. 1384–1394, Jun. 2010.
- [5] C.-H. Wu and C.-L. Chen, "High-efficiency current-regulated charge pump for a white LED driver," *IEEE Trans. Circuits Syst. II, Exp. Briefs*, vol. 56, no. 10, pp. 614–618, Oct. 2009.
- [6] P. Malcovati, M. Belloni, F. Gozzini, C. Bazzani, and A. Baschiroto, "A 0.18 μm CMOS 91%-efficiency 0.1-to-2 A scalable buck-boost DC-DC converter for LED drivers," in *Proc. ISSCC Dig. Tech. Papers*, Feb. 2012, pp. 280–281.
- [7] S. Rao, Q. Khan, S. Bang, D. Swank, A. Rao, W. McIntyre, and P. K. Hanumolu, "A 1.2 A buck-boost LED driver with 13% efficiency

- improvement using error-averaged SenseFET-Based current sensing," in *Proc. ISSCC Dig. Tech. Papers*, Feb. 2011, pp. 238–239.
- [8] S.-I. Hong, J.-W. Han, D.-H. Kim, and O.-K. Kwon, "A double-loop control LED backlight driver IC for medium-sized LEDs," in *Proc. ISSCC Dig. Tech. Papers*, Feb. 2010, pp. 116–117.
- [9] M.-H. Huang and K.-H. Chen, "Single-inductor multi-output (SIMO) DC-DC converters with high light-load efficiency and minimized cross-regulation for portable devices," *IEEE J. Solid-State Circuits*, vol. 44, no. 4, pp. 1099–1111, Apr. 2009.
- [10] E. Bonizzoni, F. Borghetti, P. Malcovati, F. Maloberti, and B. Niessen, "A 200 mA 93% peak efficiency single-inductor dual-output DC-DC buck converter," in *Proc. IEEE ISSCC Dig. Tech. Papers*, Feb. 2007, pp. 526–619.
- [11] C.-Y. Hsieh and K.-H. Chen, "Boost DC-DC converter with fast reference tracking (FRT) and charge-recycling (CR) techniques for high-efficiency and low-cost LED driver," *IEEE J. Solid-State Circuits*, vol. 44, no. 9, pp. 2568–2580, Sep. 2009.
- [12] H. Chen, Y. Zhang, and D. Ma, "A SIMO parallel-string driver IC for dimmable LED backlighting with local bus voltage optimization and single time-shared regulation loop," *IEEE Trans. Power Electron.*, vol. 27, no. 1, pp. 452–462, Jan. 2012.
- [13] D. Ma, W.-H. Ki, P. K. T. Mok, and C.-Y. Tsui, "Single-inductor multiple-output switching converters with bipolar outputs," in *Proc. IEEE Int. Symp. Circuits Syst.*, May 2001, vol. 3, pp. 301–304.
- [14] D. Ma, W.-H. Ki, C.-Y. Tsui, and P. K. T. Mok, "A 1.8 V single-inductor dual-output switching converter for power reduction techniques," in *Proc. IEEE Symp. VLSI Circuits*, Jun. 2001, pp. 137–140.
- [15] W.-H. Ki and D. Ma, "Single-inductor multiple-output switching converters," in *Proc. 32nd IEEE Power Electron. Spec. Conf.*, Jun. 2001, vol. 1, pp. 226–231.
- [16] D. Ma, W.-H. Ki, C.-Y. Tsui, and P. K. T. Mok, "Single-inductor multiple-output switching converters with time-multiplexing control in discontinuous conduction mode," *IEEE J. Solid-State Circuits*, vol. 38, no. 1, pp. 89–100, Jan. 2003.
- [17] D. Ma, W.-H. Ki, and C.-Y. Tsui, "A pseudo-CCM/DCM SIMO switching converter with freewheel switching," *IEEE J. Solid-State Circuits*, vol. 38, no. 6, pp. 1007–1014, Jun. 2003.
- [18] D. Kwon and G. A. Rincón-Mora, "Single-inductor multiple-output switching DC–DC converters," *IEEE Trans. Circuits Syst. II, Exp. Briefs*, vol. 56, no. 8, pp. 614–618, Aug. 2009.
- [19] K.-S. Seol, Y.-J. Woo, G.-H. Cho, G.-H. Gho, and J.-W. Lee, "A synchronous multioutput step-up/down DC–DC converter with return current control," *IEEE Trans. Circuits Syst. II, Exp. Briefs*, vol. 56, no. 3, pp. 210–214, Mar. 2009.
- [20] C.-W. Leng, C.-H. Yang, and C.-H. Tsai, "Digital PWM controller for SIDO switching converter with time-multiplexing scheme," in *Proc. Int. Symp. VLSI Design Autom. Test*, Apr. 2009, pp. 52–55.
- [21] Y.-J. Moon, Y.-S. Roh, J.-C. Gong, and C. Yoo, "Load-independent current control technique of a single-inductor multiple-output switching DC–DC converter," *IEEE Trans. Circuits Syst. II, Exp. Briefs*, vol. 59, no. 1, pp. 50–54, Jan. 2012.
- [22] F. Su, W.-H. Ki, and C.-Y. Tsui, "Ultra fast fixed-frequency hysteretic buck converter with maximum charging current control and adaptive for DVS applications," *IEEE J. Solid-State Circuits*, vol. 43, no. 4, pp. 815–822, Apr. 2008.
- [23] W.-H. Ki, K.-M. Lai, and C. Zhan, "Charge balance analysis and state transition analysis of hysteretic voltage mode switching converters," *IEEE Trans. Circuits Syst. I, Reg. Papers*, vol. 58, no. 5, pp. 1142–1153, May 2011.
- [24] K. K.-S. Leung and H. S.-H. Chung, "Dynamic hysteresis band control of the buck converter with fast transient response," *IEEE Trans. Circuits Syst. II, Exp. Briefs*, vol. 52, no. 7, pp. 398–402, Jul. 2005.
- [25] H. Eachempatti, S. Ganta, J. Silva-Martinez, and H. Martínez-García, "SIDO buck converter with independent outputs," in *Proc. 53rd IEEE Int. Midwest Symp. Circuits Syst.*, Aug. 2010, pp. 37–40.
- [26] F. Su and W.-H. Ki, "Digitally assisted quasi- $V^2$  hysteretic buck converter with fixed frequency and without using Large-ESR capacitor," in *Proc. ISSCC Dig. Tech. Papers*, Feb. 2009, pp. 446–447.
- [27] Cadence Spectre Circuit Simulator Datasheet [Online]. Available: [http://www.cadence.com/products/cic/spectre\\_circuit/pages/default.aspx](http://www.cadence.com/products/cic/spectre_circuit/pages/default.aspx)
- [28] M. Doshi and R. Zane, "Digital architecture for driving large LED arrays with dynamic bus voltage regulation and phase shifted PWM," in *Proc. Appl. Power Electron. Conf.*, Feb. 2007, pp. 287–293.
- [29] W.-S. Oh, D. Cho, K.-M. Cho, G.-W. Moon, B. Yang, and T. Jang, "A novel two-dimensional adaptive dimming technique of X-Y channel drivers for LED backlight system in LCD TVs," *J. Display Technol.*, vol. 5, no. 1, pp. 20–26, Jan. 2009.
- [30] Datasheet: LP8545, "LP8545 High-efficiency LED backlight driver for notebooks," Texas Instruments Incorporated, [Online] Available: <http://www.ti.com/general/docs/lit/getliterature.tsp?genericPartNumber=lp8545&fileType=pdf>
- [31] Datasheet: MAX16814, "Integrated, 4-channel, high-brightness LED driver with high-voltage DC-DC controller," Maxim Integrated Products, Inc., [Online], Available: <http://datasheets.maximintegrated.com/en/ds/MAX16814.pdf>
- [32] K. H. Loo, W. K. Lun, S. C. Tan, Y. M. Lai, and C. K. Tse, "On driving techniques for LEDs: Toward a generalized methodology," *IEEE Trans. Power Electron.*, vol. 24, no. 12, pp. 2967–2976, Dec. 2009.
- [33] W. K. Lun, K. H. Loo, S. C. Tan, Y. M. Lai, and C. K. Tse, "Bilevel current driving technique for LEDs," *IEEE Trans. Power Electron.*, vol. 24, no. 12, pp. 2920–2932, Dec. 2009.
- [34] S. C. Tan, "General n-level driving approach for improving electrical-to-optical energy-conversion efficiency of fast-response saturable lighting devices," *IEEE Trans. Ind. Electron.*, vol. 57, no. 4, pp. 1342–1353, Apr. 2010.
- [35] D. Ma and W.-H. Ki, "Fast transient PCCM switching converter with freewheel switching control," *IEEE Trans. Circuits Syst. II, Exp. Briefs*, vol. 54, no. 9, pp. 825–829, Sep. 2007.
- [36] D. Ma, W.-H. Ki, and C.-Y. Tsui, "Single-inductor multiple-output switching converters in PCCM with freewheel switching," U.S. Patent 7 432 614, Oct. 7, 2008.
- [37] Application Note: AN-1656, "Design challenges of switching LED drivers," Texas Instruments Incorporated, [Online] Available: <http://www.ti.com/general/docs/lit/getliterature.tsp?literatureNumber=snva253&fileType=pdf>
- [38] Solutions Guide, "LED drivers for high-brightness lighting," Texas Instruments Incorporated, [Online], Available: <http://www.ti.com/general/docs/lit/getliterature.tsp?baseLiteratureNumber=snvy001>
- [39] R. W. Erickson and D. Maksimovic, *Fundamentals of Power Electronics*, 2nd ed. New York, NY, USA: Springer, 2001.
- [40] Datasheet: SMD5730, "SMD 5730 White LED Datasheet," APT Electronics Ltd., [Online], Available: <http://www.appt-hk.com/en/product/?95.html>
- [41] Z. Ye, F. Greenfeld, and Z. Liang, "Design considerations of a high power factor SEPIC converter for high brightness white LED lighting applications," in *Proc. IEEE Power Electron. Spec. Conf.*, 2008, pp. 2657–2663.



**Albert T. L. Lee** received the Bachelor of Science degree in electrical engineering from the University of Wisconsin, Madison, USA, in 1994, and the Master of Science degree from the University of Michigan, Ann Arbor, USA, in 1996. He is currently working toward the Doctor of Philosophy degree in electronic and computer engineering at the Hong Kong University of Science and Technology, Kowloon, Hong Kong.

He joined Intel Corporation, Hillsboro, OR, USA, in 1996 as a Senior Component Design Engineer and was involved in the development of Intel's P6 family microprocessors. In 2001, he served as a Senior Corporate Application Engineer in the System-Level Design Group at Synopsys Inc., Mountain View, CA, USA. In 2003, he joined the Hong Kong Applied Science and Technology Research Institute Company Ltd. and served as EDA Manager in the Wireline Communications Group. In 2006, he joined the Giant Electronics Limited as Hardware Design Manager and became Associate General Manager in 2008. His research interests include mixed-signal system-level design, LED driver, power management system, and very large scale integration circuits.

867  
868  
869  
870  
871  
872  
873  
874  
875  
876  
877  
878  
879  
880  
881  
882  
883  
884  
885  
886  
887  
888  
889  
890



**Johnny K. O. Sin** (S'79–M'88–SM'96–F'12) received the B.A.Sc., M.A.Sc., and Ph.D. degrees in electrical engineering from the University of Toronto, Toronto, ON, Canada, in 1981, 1983, and 1988, respectively.

From 1988 to 1991, he was a Senior Member of the research staff of Philips Laboratories, Briarcliff Manor, NY, USA. In August 1991, he joined the Department of Electronic and Computer Engineering, The Hong Kong University of Science and Technology, Kowloon, Hong Kong, where he has been a Full

Professor since 2001. He is the holder of 13 patents, and the author of more than 270 papers in technical journals and refereed conference proceedings. His research interests include microelectronic and nanoelectronic devices and fabrication technology, particularly novel power semiconductor devices and ICs, and system-on-a-chip applications using CMOS and power transistors and silicon-embedded magnetic and capacitive devices.

Dr. Sin was an Editor for the IEEE ELECTRON DEVICES LETTERS from 1998 to 2010. He is a member of the Power Devices and IC's Technical Committee of the IEEE Electron Devices Society. He is also a Technical Committee member of the International Symposium on Power Semiconductor Devices and IC's. He is a Fellow of the IEEE for contributions to the design and commercialization of power semiconductor devices.



**Philip C. H. Chan** (SM'97–F'07) received the Bachelor of Science degree in electrical engineering from the University of California at Davis, Davis, USA, in 1973, and the Master of Science and Doctor of Philosophy degrees in electrical engineering from the University of Illinois at Urbana-Champaign, Urbana, USA, in 1975 and 1978, respectively.

He later joined Intel Corporation, Santa Clara, CA, USA, in 1981 and became a Senior Project Manager in Technology Development. He joined the Hong Kong University of Science and Technology

(HKUST) in 1991 as a founding member. He served at HKUST as the Associate Dean of Engineering and Head of the Department of Electronic and Computer Engineering. He became the Dean of Engineering in September 2003. He joined the Hong Kong Polytechnic University, Hong Kong, in 2010 as the Deputy President and Provost. His research interests include very large scale integration devices, circuits, electronic packaging, and integrated sensors.

Dr. Chan received the ECE Distinguished Alumni Award from the University of Illinois, Urbana-Champaign in 2010.

891  
892  
893  
894  
895  
896  
897  
898  
899  
900  
901  
902  
903  
904  
905  
906  
907  
908  
909  
910

IEEE  
Proof

912 Q1. Author: Please provide year information in Refs. [27], [30], [31], [37], [38], and [40].

IEEE  
Proof